Dynamics of steps along a martensitic phase boundary I: semi-analytical solution

Yubao Zhen,

School of Astronautics, Harbin Institute of Technology, Harbin, 150001, P.R. China

Anna Vainchtein *

Department of Mathematics, University of Pittsburgh, Pittsburgh, PA 15260, USA

Abstract

We study the motion of steps along a martensitic phase boundary in a cubic lattice. To enable analytical calculations, we assume antiplane shear deformation and consider a phase transforming material with a stress-strain law that is piecewise linear with respect to one component of shear strain and linear with respect to another. Under these assumptions we derive a semi-analytical solution describing a steady sequential motion of the steps under an external loading. Our analysis yields kinetic relations between the driving force, the velocity of the steps and other characteristic parameters of the motion. These are studied in detail for the two-step and three-step configurations. We show that the kinetic relations are significantly affected by the material anisotropy. Our results indicate the existence of multiple solutions exhibiting sequential step motion.

Key words: lattice model, phase boundary, interphase step, sequential motion

1 Introduction

The dissipative properties of active materials undergoing martensitic phase transitions are due to the motion of phase boundaries. Although classical nonlinear elasticity captures the main features of equilibrium microstructures

* Corresponding author. Tel.: +1 412 624 8309; Fax: +1 412 624 8397.
Email addresses: zhenyb@hit.edu.cn (Yubao Zhen), aav4@pitt.edu (Anna Vainchtein).

(see Bhattacharya (2003) for a review), it provides no information about kinetics of a phase boundary due to the inherent inability of the theory to describe phenomena in a narrow transition front where the energy dissipation occurs. This deficiency of the continuum theory renewed the interest in the discrete models of moving dislocations (Ishioka, 1971; Celli and Flytzanis, 1970; Flytzanis et al., 1974; Atkinson and Cabrera, 1965), cracks and failure waves (Slepyan, 1981, 1982; Slepyan and Troyankina, 1984; Marder and Gross, 1995) and motivated recent studies of the dynamics of lattice defects (Cahn et al., 1998; Chow, 2000; Slepyan, 2001, 2002; Kresse and Truskinovsky, 2003, 2004; Carpio and Bonilla, 2003a,b,c; Abeyaratne and Vedantam, 2003; Slepyan and Ayzenberg-Stepanenko, 2004). In particular, much of recent activity has focused on the dynamics of phase transitions in one-dimensional bistable chains (Balk et al., 2001a,b; Purohit, 2002) and derivation of a kinetic relation between the driving force on a moving phase boundary and its velocity (Slepyan et al., 2005; Truskinovsky and Vainchtein, 2005a,b, 2006).

In this paper we consider a phase boundary moving in a three-dimensional lattice. In this setting it is important that a martensitic phase boundary is typically not flat, even though it may appear so on the macrolevel. Instead, a phase boundary contains *steps*, or ledges. A long-standing hypothesis in materials science is that a phase boundary moves forward via a propagation of steps *along* the interface (Hirth and Lothe, 1982; Hirth, 1994). This hypothesis is confirmed by experimental observations: for example, Bray and Howe (1996) found the fcc/hcp martensite transformation in Co-Ni occurs by the passage of Shockley partial dislocation ledges and that the hcp martensite thickens by the lateral movement of ledges across the fcc/hcp interface. Thus kinetics of a phase boundary is largely determined by the kinetics of the steps. In this paper we focus on the dynamics of multiple steps along a phase boundary.

Intuitively, it is clear that simultaneous motion of several steps is not energetically favorable. In fact, calculations of Sharma and Vainchtein (2007) for a quasistatic stepped phase boundary show that a *sequential* one-by-one propagation of steps involves significantly smaller energy barriers than simultaneous motion. Numerical simulations presented in the second part of this paper (Zhen and Vainchtein, 2007), henceforth referred to as Part II, show that the sequential propagation of steps is also preferred in dynamics. In most simulations the steps propagate with the same average velocity, but there are time delays between the step advancements. In this paper we construct a semi-analytical solution describing this type of motion. Specifically, we consider a phase boundary with an arbitrary finite number of steps in a cubic lattice subjected to an antiplane shear deformation. One may view this setup as a discrete analog of a twinning step considered by Tsai and Rosakis (2001). The nonconvex interaction potential governing the bonds in one direction has three convex quadratic regions, with the central region representing the parent austenite phase, and the two symmetric parabolas representing two variants

of the martensite phase. To model material anisotropy, the interaction in the orthogonal direction is assumed to be harmonic with an elastic modulus that may be different from the phase-transforming bonds. These assumptions yield an explicit expression for the motion of steps, up to some integrals that need to be evaluated numerically. We obtain the kinetic relations between the driving force and the parameters of the motion. These relations are multivalued, suggesting that multiple solutions of this type may coexist at the same velocity or driving force, as confirmed by the results of simulations presented in Part II. The cases of two and three steps are studied in detail, and uniform asymptotic approximations of the solutions are obtained.

The kinetic relations we obtain for the propagation of two steps are similar to the ones describing the motion of two screw dislocations on the same slip plane studied by Flytzanis et al. (1974). This similarity is not surprising in view of a close connection between dislocations and ledges (Olson and Cohen, 1979; Christian, 1994). In fact, after a few simple modifications the solution obtained in this paper may be used to describe the motion of an arbitrary number of dislocations located on neighboring slip planes. However, there are some important differences. In particular, the dislocation model assumes a periodic potential, which results in the breakdown of a steady dislocation motion at a sufficiently high subsonic velocity (Flytzanis et al., 1974) and leads to nucleation of new dislocations on the same slip plane (Koizumi et al., 2002). Meanwhile, the three-parabola potential used here to model the phase transition delays the breakdown of steady subsonic motion. Moreover, we identify parameter regimes in which the steady motion does not break down until the velocity reaches a certain supersonic value, so that a steady supersonic motion of steps becomes possible. The analysis in this paper and numerical simulations in Part II show that the nucleation of new steps takes place at a near-sonic critical speed, with the new steps forming on top of the existing ones, as predicted by Ishioka (1975). In addition, unlike the dislocation model, the model considered here allows for the austenite and martensite potential wells to be of different height, and in general the two phases may have different elastic moduli, although only the equal moduli case is considered here to simplify the calculations. Finally, the current model incorporates the elastic anisotropy which is shown to have a significant effect on kinetic relations. In particular, anisotropy alters the critical velocity at which the steady step motion breaks down: if the harmonic bonds are sufficiently strong, it becomes supersonic, making supersonic steady motion possible; while the weaker bonds lead to step nucleation in the subsonic regime already. In addition, we show that stiffer harmonic bonds result in a larger separation between the moving steps and a lower driving force needed for the steps to move with the same velocity.

The first part of this paper is organized as follows. Section 2 introduces the antiplane shear lattice model. In Section 3 we derive the general solution

and obtain the kinetic relations for a phase boundary with a finite number of steps. A detailed analysis of alternate motion of two steps is presented in Section 4, and the sequential motion of three steps is considered in Section 5. In Section 6 we find the critical velocities at which the steady step motion breaks down. The work is summarized in Section 7. Derivation of the expression for the driving force can be found in Appendix A, and Appendix B contains asymptotic expressions for the obtained subsonic solutions.

2 The antiplane shear lattice model

Consider a three-dimensional cubic lattice with the orthonormal basis $\{\mathbf{e}_1, \mathbf{e}_2, \mathbf{e}_3\}$ undergoing an antiplane shear deformation. This means that the atomic rows along $\mathbf{e}_3$-direction are rigid and can move only along their length. The problem thus reduces to an out-of-plane deformation of a two-dimensional square lattice spanned by the vectors $\mathbf{e}_1$ and $\mathbf{e}_2$ and consisting of particles of mass M located at $(m\varepsilon, n\varepsilon)$, where $(m, n) \in \mathbb{Z}^2$ and ε is the lattice spacing. The displacement of (m, n)th particle at time t is $U_{m,n}(t)\mathbf{e_3}$. The deformation of the lattice is measured by the horizontal strain

$$w_{m,n} = \frac{U_{m,n} - U_{m-1,n}}{\varepsilon} \tag{1}$$

and the vertical strain

$$v_{m,n} = \frac{U_{m,n} - U_{m,n-1}}{\varepsilon} \tag{2}$$

at each particle. We assume that each particle interacts with its four nearest neighbors. The interaction forces due to the neighboring particles in the horizontal and vertical directions are denoted by $F_{\mathrm{h}}(w)$ and $F_{\mathrm{v}}(v)$, respectively, where w and v denote the horizontal and vertical strains defined above.

To model a martensitic phase transformation, we will assume that the interaction in the vertical bonds is governed by a nonconvex potential $\Phi_{\mathrm{v}}(v)$ with three convex regions, as shown in Fig. 1. The central convex region represents the austenite phase (phase I), and the two other model the symmetry-related variants of martensite (phase II). To enable analytical calculations, we will assume that each convex region is a parabola, so that the interaction force $F_{\mathrm{v}}(v) = \Phi'_{\mathrm{v}}(v)$ is piecewise linear:

$$F_{\mathrm{v}}(v) = K_{\mathrm{V}}(v - a\theta(|v| - v_c)\mathrm{sgn}(v)), \tag{3}$$

where $\theta(x)$ is the unit step function ($\theta(x) = 1$ if $x \geq 0$ and zero otherwise). Thus each vertical bond can exist in two different phases depending on whether the magnitude of vertical strain v is below (phase I) or above (phase II) the critical value v_c. Here $K_{\mathrm{V}} > 0$ is the elastic modulus in each phase and $a > 0$

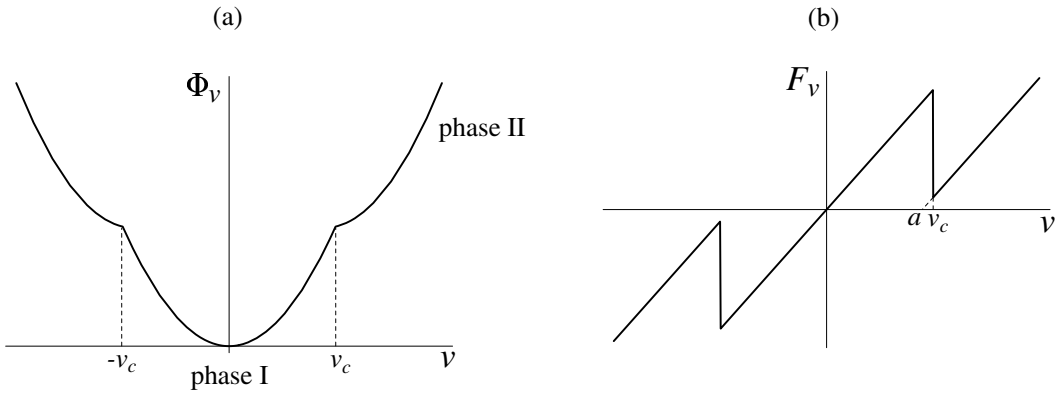

Fig. 1. Interaction potential (a) and force (b) in the vertical bonds.

denotes the transformation strain (distance between the two adjacent linear branches); note that a and v_c are generally independent. The interaction in the horizontal bonds is assumed to be linear:

$$F_{\rm h}(w) = K_{\rm H} w, \tag{4}$$

with positive elastic modulus $K_{\rm H} > 0$.

The motion of the lattice is governed by the infinite system of ordinary differential equations

$$\begin{aligned} M\ddot{U}_{m,n} =& F_{\rm h}\left(\frac{U_{m+1,n}-U_{m,n}}{\varepsilon}\right) - F_{\rm h}\left(\frac{U_{m,n}-U_{m-1,n}}{\varepsilon}\right) \\ &+ F_{\rm v}\left(\frac{U_{m,n+1}-U_{m,n}}{\varepsilon}\right) - F_{\rm v}\left(\frac{U_{m,n}-U_{m,n-1}}{\varepsilon}\right), \end{aligned} \tag{5}$$

where $(m,n) \in \mathbb{Z}^2$. It is convenient to introduce dimensionless variables

$$u = \frac{U}{\varepsilon}, \quad \tau = t\sqrt{\frac{K_{\rm V}}{M\varepsilon}}, \quad f_{\rm h} = \frac{F_{\rm h}}{K_{\rm V}}, \quad f_{\rm v} = \frac{F_{\rm v}}{K_{\rm V}}. \tag{6}$$

Note that in the new variables the strains in the horizontal and vertical bonds are given by $w_{m,n} = u_{m,n} - u_{m-1,n}$ and $v_{m,n} = u_{m,n} - u_{m,n-1}$, respectively; and the force-strain relationships become

$$f_{\rm h}(w) = \chi w, \tag{7}$$

$$f_{\rm v}(v) = v - a\theta(|v| - v_c)\mathrm{sgn}(v), \tag{8}$$

where $\chi \equiv K_{\rm H}/K_{\rm V}$ is the dimensionless parameter measuring relative strength of the moduli in the two directions of the lattice. The dimensionless equations of motion then reduce to

$$\begin{aligned} \ddot{u}_{m,n} =& \chi(u_{m+1,n} - 2u_{m,n} + u_{m-1,n}) + (u_{m,n+1} - 2u_{m,n} + u_{m,n-1}) \\ &- a\{\mathrm{sgn}(u_{m,n+1} - u_{m,n})\theta(|u_{m,n+1} - u_{m,n}| - v_c) \\ &- \mathrm{sgn}(u_{m,n} - u_{m,n-1})\theta(|u_{m,n} - u_{m,n-1}| - v_c)\}. \end{aligned} \tag{9}$$

Observe that in each phase the equation is linear and admits the plane wave solutions of the form $u_{m,n} = A\exp(i(\omega t + mk_x + nk_y))$, where the wave frequency ω must satisfy the dispersion relation

$$\omega^2 = 4\left(\chi \sin^2 \frac{k_x}{2} + \sin^2 \frac{k_y}{2}\right). \tag{10}$$

3 General solution for a multiple step configuration

Suppose now that a phase boundary divides the lattice into two regions, as shown in Fig. 2. The vertical bonds in the lower region (shaded area) are in phase II (high-strain phase, $v > v_c$), while in the upper region the bonds are in the low-strain phase I ($|v| < v_c$). We assume that the phase boundary consists of N steps, or ledges. Outside the step zone, the phase boundary is flat and extends to infinity on both sides. Suppose now that each step moves

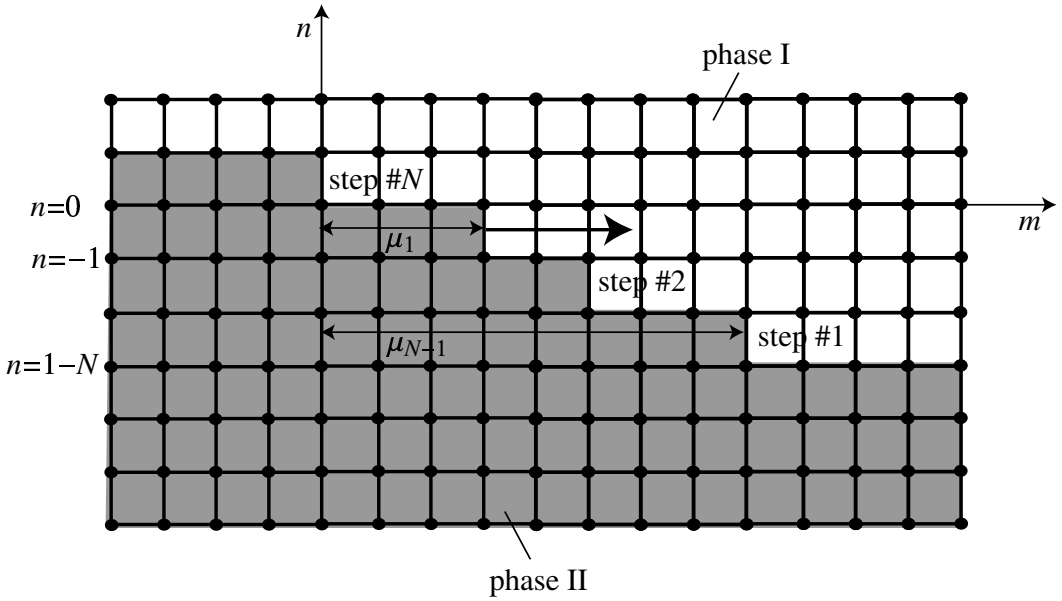

Fig. 2. A phase boundary with N steps (here $N = 4$). Vertical bonds are in phase II in the shaded region and in phase I in the rest of the lattice.

with a constant average velocity V from left to right but the steps do not necessarily move simultaneously. Instead, we will assume the following motion of the steps. At the time $\tau = 0$, the front of the highest Nth step coincides with $(0, 1)$th vertical bond, which has transformed from phase I to a phase II, while the jth step, $j = 1, \ldots, N$, stays $\mu_{N-j} \in \mathbb{N}$ lattice spaces ahead at the $(\mu_{N-j}, 1-N+j)$th vertical bond. At $\tau = T_j < 1/V$, the jth step moves forward by one lattice spacing, via the transformation of $(\mu_{N-j}+1, 1-N+j)$th vertical bond to phase II. By the time $\tau = 1/V$ all steps have moved forward by one lattice spacing, and the motion pattern repeats periodically. Obviously, $\mu_0 = 0$

and $T_N = 1/V$. If the times T_j, $j = 1, \ldots, N$ are all distinct and nonzero, the steps move one after another, or *sequentially*, with a time delay between their motions. Note that the order in which the steps move is not predetermined and need not coincide with the reverse order of the steps. We assume that T_j are constant throughout the motion.

Assuming the motion described above, we can rewrite Eq. (9) as

$$\ddot{u}_{m,n} = \chi(u_{m+1,n} + u_{m-1,n} - 2u_{m,n}) + (u_{m,n+1} + u_{m,n-1} - 2u_{m,n}) + a\left[\delta_{n,1-N} + \sum_{p=0}^{N-1}(\delta_{n,1-p} - \delta_{n,-p})\rho(m - V\tau - \alpha_p)\right], \quad (11)$$

where

$$\alpha_p = \mu_p + 1 - VT_{N-p}, \quad p = 0, \ldots, N-1 \quad (12)$$

is the dynamic separation between the $(N-p)$th and Nth step (note that $\alpha_0 = 0$). The function $\rho(x) = 1 - \theta(x)$ is the complementary unit step function ($\rho(x) = 1$ for $x < 0$ and $\rho(x) = 0$ otherwise) and $\delta_{m,n}$ is the Kronecker delta function.

We seek solution of Eq. (11) in the form of a traveling wave:

$$u_{m,n}(\tau) = u(\xi, n), \qquad \xi = m - V\tau. \quad (13)$$

We assume that at infinity the vertical strain $v(\xi, n) = u(\xi, n) - u(\xi, n-1)$ tends to constant values $v_+ < v_c$ and $v_- > v_c$ in phase I and II, respectively:

$$\begin{aligned} &\text{as } n \to \pm\infty, \quad v(\xi, n) \to v_\pm, \\ &\text{as } \xi \to \pm\infty, \quad v(\xi, n) \to \begin{cases} v_+, & n \geq 2 \\ v_\pm, & n = 2-N, \ldots, 1 \\ v_-, & n \leq 1-N. \end{cases} \end{aligned} \quad (14)$$

In addition, we require that whenever each step moves to its next location, the phase switch takes place:

$$v(\alpha_{1-n}, n) = v_c, \qquad n = 2-N, \ldots, 1; \quad (15)$$

while the vertical bonds behind and in front of the step-like phase boundary, as well as those outside the step zone remain in their respective phases:

$$\begin{aligned} &v(\xi, n) \gtrless v_c, \quad \xi \lessgtr \alpha_{1-n}, \quad n = 2-N, \ldots, 1, \\ &v(\xi, n) < v_c, \quad n \geq 2, \\ &v(\xi, n) > v_c, \quad n \leq 1-N. \end{aligned} \quad (16)$$

We also assume that $v > -v_c$ in all vertical bonds.

The problem thus consists of using the ansatz (13) to solve Eq. (11) subject to the conditions (14–16). Not surprisingly, the problem is similar to the ones encountered in the studies of screw dislocations (Celli and Flytzanis, 1970; Ishioka, 1971; Flytzanis et al., 1974). In fact, by principle of superposition its solution can be represented as the sum of solution of the problem with a flat phase boundary and the sum of solutions due to N screw dislocations located at the step fronts. More precisely, we write

$$u(\xi, n) = u_n^S + \sum_{p=0}^{N-1} u_p^D(\xi, n). \tag{17}$$

Here

$$u_n^S = \begin{cases} (n-1+N)(v_- - a), & n \geq 1-N, \\ (n-1+N)v_-, & n \leq -N, \end{cases} \tag{18}$$

is a time-independent solution of static problem with the flat interface along $n = 1 - N$ line:

$$0 = u_{n+1}^S + u_{n-1}^S - 2u_n^S + a\delta_{n,1-N}. \tag{19}$$

Note that it satisfies the boundary conditions (14) for $n \neq 2 - N, \ldots, 1$ with the far-field strains $v_\pm$ related by

$$v_- - v_+ = a. \tag{20}$$

Meanwhile, $u_p^D(\xi, n)$, $p = 0, \ldots, N-1$, in Eq. (17) solves the dynamic problem due to the screw dislocation located between the lines $n = -p$ and $n = 1 - p$:

$$\begin{aligned} V^2 \frac{\partial^2 u_p^D(\xi, n)}{\partial \xi^2} &= \chi(u_p^D(\xi+1, n) + u_p^D(\xi-1, n) - 2u_p^D(\xi, n)) + u_p^D(\xi, n+1) \\ &+ u_p^D(\xi, n-1) - 2u_p^D(\xi, n) + a(\delta_{n,1-p} - \delta_{n,-p})\rho(\xi - \alpha_p). \end{aligned} \tag{21}$$

Due to Eqs. (17), (18), (20) and (14), $v_p^D(\xi, n) = u_p^D(\xi, n) - u_p^D(\xi, n-1)$ tends to zero as $|n| \to \infty$ (for any ξ) and as $|\xi| \to \infty$ for $n \neq 1 - p$, while

$$v_p^D(\xi, 1-p) \to \begin{cases} a, & \xi \to -\infty, \\ 0, & \xi \to \infty. \end{cases} \tag{22}$$

As in Celli and Flytzanis (1970), we apply discrete Fourier transform in n followed by continuous Fourier transform in ξ to Eq. (21), obtaining

$$u_p^D(\xi, n) = \frac{a}{4\pi^2} \int_{-\infty}^{\infty} \frac{e^{ik_\xi(\alpha_p - \xi)}}{ik_\xi} \mathcal{T}(n+p, k_\xi) \mathrm{d}k_\xi, \tag{23}$$

where we defined, for any integer j,

$$\mathcal{T}(j, k_\xi) = \int_{-\pi}^{\pi} \frac{(1 - e^{ik_y})}{V^2 k_\xi^2 - 4(\chi \sin^2 \frac{k_\xi}{2} + \sin^2 \frac{k_y}{2})} e^{-ik_y j} \mathrm{d}k_y. \tag{24}$$

Note that $\mathcal{T}(j, k_\xi)$ has the symmetry property

$$\mathcal{T}(-j, k_\xi) + \mathcal{T}(j+1, k_\xi) = 0, \quad j \in \mathbb{Z}, \tag{25}$$

and hence only needs to be evaluated for $j \geq 1$. Following Celli and Flytzanis (1970), we define the function

$$\lambda(k_\xi) = 1 + 2\chi \sin^2 \frac{k_\xi}{2} - \frac{1}{2} V^2 k_\xi^2, \tag{26}$$

and let z be a complex number given by $z \equiv e^{ik_y}$. Then the integral (24) can be rewritten as

$$\mathcal{T}(j, k_\xi) = \oint_{|z|=1} \frac{(1-z)z^{-j}}{i(z^2 - 2\lambda z + 1)} \mathrm{d}z. \tag{27}$$

Note that it depends on k_ξ through $\lambda = \lambda(k_\xi)$ defined in Eq. (26). In order to evaluate $\mathcal{T}(j, k_\xi)$, we need to determine the poles of the integrand in Eq. (27). One can see that when $|\lambda| \neq 1$ there are two poles. For $|\lambda| > 1$, both poles are real and given by $\lambda \pm \sqrt{\lambda^2 - 1}$, one inside the unit circle and the other outside. For $|\lambda| < 1$, these two poles are $\lambda \pm i\sqrt{1 - \lambda^2}$, which are complex numbers and lie on the unit circle (the path of integration). Here we use the causality condition (Papoulis, 1962) requiring the inverse transform function to be causal to determine how the path is indented. This is described below.

When $\xi > 0$, we can evaluate the inverse Fourier transform on the right hand side of Eq. (23) by closing the contour in the lower half k_ξ-complex plane. The causality condition requires that at $\tau \to -\infty$, which corresponds to $\xi \to +\infty$, the recovered function vanishes. This means all the possible poles on the k_ξ axis should be treated as belonging to the upper half plane, which is equivalent to shifting the path of integration below the poles, i.e., $k_\xi \mapsto k_\xi - i\epsilon$, where ϵ is a small positive real number. The causality condition is then satisfied due to a factor of $e^{-\epsilon\xi}$ in the integrand.

Replacing k_ξ by $k_\xi - i\epsilon$ in Eq. (26), we have

$$\lambda(k_\xi - i\epsilon) \approx \lambda(k_\xi) - i\epsilon\lambda'(k_\xi), \tag{28}$$

so that

$$|\lambda \pm i\sqrt{1 - \lambda^2}|^2 \approx 1 \mp 4\epsilon\lambda'(k_\xi). \tag{29}$$

Hence when $\lambda'(k_\xi) > 0$, the pole $z = \lambda - i\sqrt{1 - \lambda^2}$ is approached from outside the unit circle as $\epsilon \to 0+$, while the pole $z = \lambda + i\sqrt{1 - \lambda^2}$ is approached from inside the circle in this limit. Thus we need to replace the unit circle contour in Eq. (27) by a new contour Γ, which coincides with $|z| = 1$ everywhere except near the pole $z = \lambda - i\sqrt{1 - \lambda^2}$, where the circle is indented inward (so that the pole is outside the circle) and the pole $z = \lambda + i\sqrt{1 - \lambda^2}$, where the circle is indented outward. Similarly, when $\lambda'(k_\xi) < 0$, the poles $z = \lambda \pm i\sqrt{1 - \lambda^2}$ are approached from outside/inside the unit circle, respectively. In this case

the new contour Γ is obtained by indenting the unit circle outward near $z = \lambda - i\sqrt{1-\lambda^2}$ and inward near $z = \lambda + i\sqrt{1-\lambda^2}$.

Consider now the region in the complex plane bounded by the contour Γ (the indented unit circle) and the circle $|z| = R$ with radius $R \to \infty$. Note that for a given nonzero k_ξ only one pole is located inside the region. Applying the residue theorem to this region, we obtain

$$\mathcal{T}(j,k_\xi) = \begin{cases} \pi(1+\sqrt{\frac{\lambda-1}{\lambda+1}})(\lambda-\sqrt{\lambda^2-1})^{-j}, & \lambda < -1 \\ \pi(1 \mp i\sqrt{\frac{1-\lambda}{1+\lambda}})(\lambda \mp i\sqrt{1-\lambda^2})^{-j}, & |\lambda|<1, \ \ \lambda'(k_\xi) \gtrless 0 \\ \pi(1+\sqrt{\frac{\lambda-1}{\lambda+1}})(\lambda+\sqrt{\lambda^2-1})^{-j}, & \lambda > 1 \end{cases} \qquad (j \geq 1). \tag{30}$$

Using the symmetry relation in Eq. (25), we can obtain $\mathcal{T}(j,k_\xi)$ for any integer j. Note that $\mathcal{T}$ is continuous across $\lambda = 1$, which includes $k_\xi = 0$. In particular, $\mathcal{T}(j,0) = \pi$ for $j \geq 1$. Clearly, the function is discontinuous across $\lambda = -1$.

Using Eqs. (17), (18), (23), (25) and (30), we obtain the vertical strain for a general N-step configuration at (ξ, n) as

$$v(\xi,n) = \frac{a}{2\pi}\int_{-\infty}^{\infty} \frac{e^{-ik_\xi\xi}}{ik_\xi}\left(\sum_{p=0}^{N-1} e^{ik_\xi\alpha_p}\mathcal{S}(n+p-1,k_\xi)\right)\mathrm{d}k_\xi + \begin{cases} v_+, \ n \geq 2-N, \\ v_-, \ n \leq 1-N, \end{cases} \tag{31}$$

where we defined

$$\mathcal{S}(j,k_\xi) = \frac{\mathcal{T}(j+1,k_\xi) - \mathcal{T}(j,k_\xi)}{2\pi}. \tag{32}$$

With Eqs. (25) and (30), Eq. (32) yields for $j \in \mathbb{Z}$

$$\mathcal{S}(j,k_\xi) = \begin{cases} (\lambda-\sqrt{\lambda^2-1})^{-|j|}(\delta_{j,0} - \sqrt{\frac{\lambda-1}{\lambda+1}}), & \lambda < -1 \\ (\lambda \mp i\sqrt{1-\lambda^2})^{-|j|}(\delta_{j,0} \pm i\sqrt{\frac{1-\lambda}{1+\lambda}}), & |\lambda|<1, \ \ \lambda'(k_\xi) \gtrless 0 \\ (\lambda+\sqrt{\lambda^2-1})^{-|j|}(\delta_{j,0} - \sqrt{\frac{\lambda-1}{\lambda+1}}), & \lambda > 1. \end{cases} \tag{33}$$

We now define

$$g_L(\xi) = \frac{1}{2\pi}\int_{-\infty}^{\infty} \frac{e^{-ik_\xi\xi}}{ik_\xi}\mathcal{S}(L,k_\xi)\mathrm{d}k_\xi, \qquad L = 0,1,\ldots \tag{34}$$

The expression (31) for the total vertical strain then simplifies to

$$v(\xi,n) = a\sum_{p=0}^{N-1} g_{|n+p-1|}(\xi-\alpha_p) + \begin{cases} v_+, \ n \geq 2-N, \\ v_-, \ n \leq 1-N. \end{cases} \tag{35}$$

This shows that the overall contribution of a specific $(N-p)$th step, $p = 0, \ldots, N-1$, to the nth layer of vertical bonds depends only on their relative vertical distance $L = |n+p-1|$ via the interaction function $g_L(\xi)$. The interaction functions can be found from numerical evaluation of the the integral in Eq. (34); their asymptotic approximations are given in Appendix B.

To determine the motion parameters, we need to require that the following phase switch conditions are satisfied at the steps:

$$v(\alpha_{1-n}, n) = v_+ + a \sum_{p=0}^{N-1} g_{|n+p-1|}(\alpha_{1-n} - \alpha_p) = v_c \qquad n = 2-N, \ldots, 1. \quad (36)$$

This system of N equations defines the *kinetic relations* between the *driving force*

$$G = a(F - F_{\mathrm{M}}) = a(v_+ - v_c + a/2) \quad (37)$$

and the N motion parameters: the velocity V of each step and the separation parameters α_j, $j = 1, \ldots, N-1$. In Eq. (37) $F = v_+$ is the applied force and $F_{\mathrm{M}} = v_c - a/2$ is the Maxwell force dividing the graph of $f_{\mathrm{v}}(v)$ into two equal areas. The derivation of (37) can be found in Appendix A. Note that Eq. (36) can be rewritten as

$$\sum_{p=0}^{N-1} (g_{|n+p|}(\alpha_{-n} - \alpha_p) - g_{|n+p-1|}(\alpha_{1-n} - \alpha_p)) = 0, \qquad n = 2-N, \ldots, 0, \quad (38)$$

a system of $N-1$ equations for α_j, $j = 1, \ldots, N-1$, and

$$\frac{G}{a^2} = \frac{1}{2} - \sum_{p=0}^{N-1} g_{|n+p-1|}(\alpha_{1-n} - \alpha_p), \quad (39)$$

expressing the driving force in terms of α_j and V. The last equality holds for any integer n such that $2 - N \le n \le 1$.

For a particular set of motion parameters satisfying Eq. (36), a solution is obtained from Eq. (35). In Appendix B we verify that this solution satisfies the conditions (14) at infinity. Finally, one needs to check that the obtained solution is consistent with our assumptions about phase distribution, i.e. that the conditions (16) are satisfied.

4 Alternate motion of two steps

As the simplest example, we will consider a two-step configuration ($N = 2$). In this case sequential motion reduces to an alternate one, with $\alpha \equiv \alpha_1$ measuring the separation between the two steps in the moving frame.

The total vertical strain (35) reduces in this case to

$$v(\xi,n) = a(g_{|n-1|}(\xi) + g_{|n|}(\xi-\alpha)) + \begin{cases} v_+, \, n \geq 0, \\ v_-, \, n \leq -1. \end{cases} \tag{40}$$

In particular, the strains in the vertical bonds at $n = 0$ and $n = 1$ (where the steps are located) are given by

$$v(\xi,0) = v_+ + a(g_0(\xi-\alpha) + g_1(\xi)), \tag{41}$$
$$v(\xi,1) = v_+ + a(g_0(\xi) + g_1(\xi-\alpha)). \tag{42}$$

Recalling Eq. (34), we obtain

$$g_0(\xi) = \frac{1}{2\pi} \int\limits_{-\infty}^{\infty} \frac{F(\lambda)}{ik_\xi} e^{-ik_\xi \xi} \mathrm{d}k_\xi, \tag{43}$$

$$g_1(\xi) = \frac{1}{2\pi} \int\limits_{-\infty}^{\infty} \left(\frac{\lambda F(\lambda) - 1}{ik_\xi} \right) e^{-ik_\xi \xi} \mathrm{d}k_\xi, \tag{44}$$

$$F(\lambda) = 1 - \left| \frac{\lambda - 1}{\lambda + 1} \right|^{\frac{1}{2}} \exp\left(\frac{\pi i}{2} (\theta(\lambda - 1) - \theta(\lambda + 1)) \mathrm{sgn}\lambda'(k_\xi) \right). \tag{45}$$

Recall that λ is a function of k_ξ defined in Eq. (26).

Note that the integrand in $g_0(\xi)$ (but not $g_1(\xi)$) has a simple pole at $k_\xi = 0$. Therefore, this integral should be understood in the principal value sense. Using causality condition, we resolve this singularity by deforming the contour of integration near $k_\xi = 0$ so that the contour goes below this point along a semi-arch with radius $r \to 0$. In addition, at each V there is a finite number of branch points along both contours that correspond to $\lambda = \pm 1$. To see this, consider the curves obtained by solving the equations $\lambda = 1$ and $\lambda = -1$ for V as a function of k_ξ. By symmetry, if k_ξ is a branch point, so is $-k_\xi$, and hence it suffices to show only the positive roots. The curves of roots are shown in Fig. 3. For each velocity V, the roots are the intersections of the curves with the horizontal line $V = \text{const}$. Observe that the lower curve, $\lambda = 1$ is bounded and has the maximum value $V = c$ at $k_\xi = 0$. Here

$$c = \sqrt{\chi} \tag{46}$$

is the long-wavelength (macroscopic) sound speed of elastic shear waves in the horizontal direction, the direction of the step motion. If the motion of the steps is *supersonic* ($V > c$), there is only one positive branch point $k_\xi = k_-$, and it corresponds to $\lambda = -1$. In the *subsonic* regime ($V < c$) there is an infinite number of critical speeds V_j^+ (dashed lines in Fig. 3) and V_j^- (solid horizontal lines), $j = 1, 2, \ldots$, that correspond to the local extrema of the curves $\lambda = 1$ and $\lambda = -1$, respectively. One can show that at the critical speeds V_j^- (where

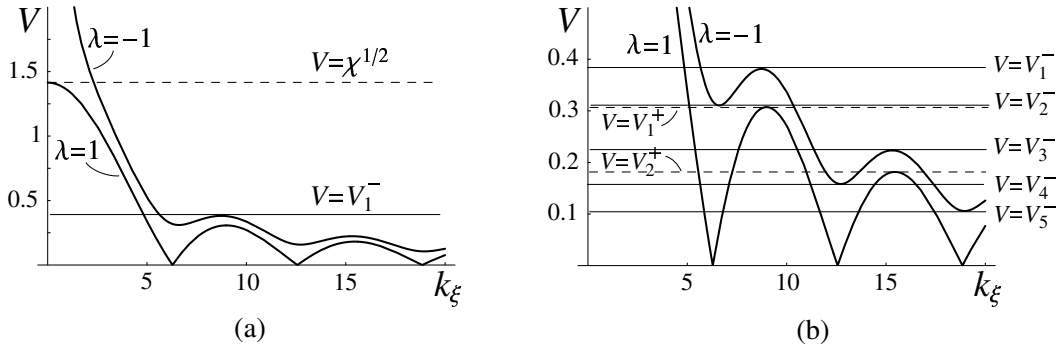

Fig. 3. (a) The roots k_ξ of $\lambda = 1$ (lower curve) and $\lambda = -1$ (upper curve). For given velocity, the roots are given by the intersections of the curves with $V = \text{const}$. (b) The same picture zoomed to show the critical velocities V_j^+ and V_j^-. Due to symmetry, only positive roots are shown.

$\lambda = -1$ and $\lambda'(k_\xi) = 0$), the integrand behaves like $1/|k_\xi - k_j^-|$ near the associated critical branch point $k_\xi = k_j^-$. Thus these velocities correspond to *resonant* states with a logarithmic singularity. In contrast, the critical speeds V_j^+ ($\lambda = 1$ and $\lambda'(k_\xi) = 0$) are merely the bifurcation points at which two adjacent roots merge into one, while the behavior of the system is continuous. Between each pair of critical speeds, there is an odd number of positive roots for each equation.

A direct semi-numerical integration can be performed at all the speeds where the system is away from resonance. One can show that the contribution of the semi-arch of radius $r \to 0$ below the pole $k_\xi = 0$ (for g_0) equals $1/2$. For very large $|k_\xi|$, asymptotic expressions of the integrands enables the analytical evaluation of the contribution to infinity in terms of cosine and sine-integral functions. We can also obtain asymptotes of the integral of the $\sqrt{|(\lambda-1)/(\lambda+1)|}$ part near the non-zero branch points. Near the branch points k_+ that correspond to $\lambda = 1$ the integrand behaves as $\sqrt{|k_\xi - k_+|}$, while near the branch points k_-, where $\lambda = -1$, the singular part of the integrand behaves as $1/\sqrt{|k_\xi - k_-|}$. Hence for $\Delta > 0$ sufficiently small we have the following approximations:

$$\pm \int_{k_+}^{k_+ \pm \Delta} e^{-ik_\xi \xi} \frac{|\frac{\lambda-1}{\lambda+1}|^{1/2}}{ik_\xi} \mathrm{d}k_\xi \approx e^{-ik_+\xi} \frac{\sqrt{\frac{|\lambda'(k_+)|}{2}}}{ik_+} \int_0^\Delta e^{\mp ix\xi} \sqrt{x} \mathrm{d}x, \tag{47}$$

$$\pm \int_{k_-}^{k_- \pm \Delta} e^{-ik_\xi \xi} \frac{|\frac{\lambda-1}{\lambda+1}|^{1/2}}{ik_\xi} \mathrm{d}k_\xi \approx e^{-ik_-\xi} \frac{\sqrt{\frac{2}{|\lambda'(k_-)|}}}{ik_-} \int_0^\Delta e^{\mp ix\xi} \frac{1}{\sqrt{x}} \mathrm{d}x. \tag{48}$$

which can all be evaluated in terms of Fresnel cosine and sine functions.

The integrals over the remaining domain (outside the branch points and, for $g_0(\xi)$, the pole at zero) are evaluated numerically. Let d be smaller than the first non-zero root of $\lambda = \pm 1$. Then on the finite range $(-d, -r) \cup (r, d)$ outside

the pole $k_\xi = 0$, the integral with the oscillatory kernel can be evaluated using the method of Capobianco and Criscuolo (2003). The remaining parts of the integrals can be obtained by the generalized Filon's method (Filon (1928–29); Flinn (1960); Iserles and Nørsett (2005)) for oscillatory integrands.

Based on the above analysis, for a given χ and a velocity V of the front, the functions $g_0(\xi)$ and $g_1(\xi)$ can be evaluated for any ξ from Eqs. (43) and (44). However, to get the vertical strain (40), we need to first determine α and G (and thus $v_\pm$ from Eqs. (20) and (37)). In this case Eqs (38) and (39) reduce to

$$g_1(\alpha) = g_1(-\alpha), \tag{49}$$

$$\frac{G}{a^2} = \frac{1}{2} - g_0(0) - g_1(\alpha). \tag{50}$$

The vertical strains in the layers containing the steps are then readily obtained from Eqs. (41) and (42). The strains in the other layers can be found using the same methods from the general formula (40).

4.1 Kinetic relations

For given values of step velocity V and parameter χ, we can solve Eq. (49) for the values of α, the dynamic separation between the two steps. Each solution corresponds to a particular value of the driving force G found using Eq. (50). Thus, we obtain the *kinetic relations* $G = G(V)$ and $\alpha = \alpha(V)$. Since the functions $g_0(\xi)$ and $g_1(\xi)$ only depend on χ and V, the kinetic relations depend only on χ. Recall that this dimensionless parameter measures the shear strength of the linearly elastic horizontal bonds relative to the vertical ones.

In what follows, we will consider the velocities above the first resonance speed: $V > V_1^-$. Recall that in this case, by Eq. (34), there are either two positive branch points, one with $\lambda = 1$ and one with $\lambda = -1$, in the subsonic case ($V < c$, with c given by Eq. (46)), or only one, with $\lambda = -1$, in the supersonic regime ($V > c$). In both cases the branch points contribute oscillations in the functions $g_0(\xi)$ and $g_1(\xi)$ only behind the moving front ($\xi < 0$), while ahead of it both functions monotonically tend to zero. Fig. 4 depicts the typical behavior of $g_0(\xi)$ and $g_1(\xi)$ in subsonic ($V = 0.833$) and supersonic ($V = 1.25$) regimes of step propagation in the absence of anisotropy ($\chi = 1$).

To compute the kinetic relations, we first solve Eq. (49) numerically for roots of $\alpha > 0$ for given $V > V_1^-$ and χ. As can be seen from Fig. 4, this equation has a large number of roots due to the oscillatory nature of $g_1(\xi)$ at $\xi < 0$. Connecting the first nonzero roots at different V/c, we obtain the first branch of $\alpha(V)$. Similarly, the set of second roots forms the second branch, and so

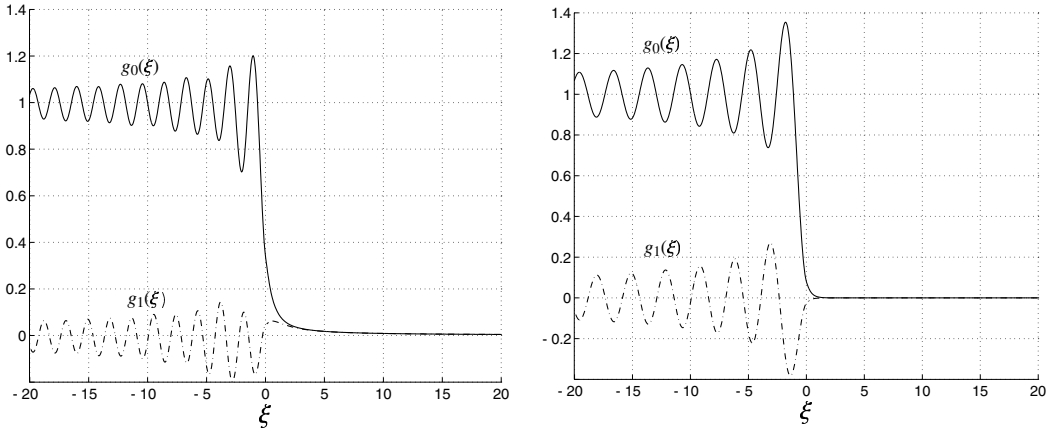

(a) subsonic, $V = 0.833$ (b) supersonic, $V = 1.25$

Fig. 4. The functions $g_0(\xi)$ and $g_1(\xi)$ for two velocities. Here $\chi = 1$.

on. The first ten branches of $\alpha(V)$ at $\chi = 1$ (which corresponds to $V_1^-/c = 0.3158$) are shown in Fig. 5. Similar results with multiple solution branches

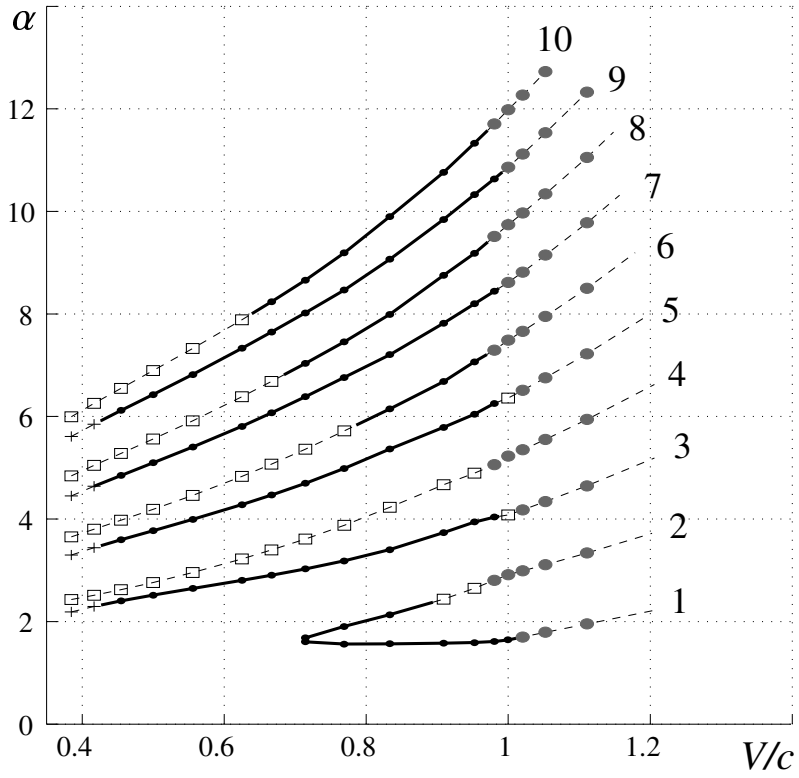

Fig. 5. The first ten branches of the kinetic relation $\alpha(V)$ at $\chi = 1$. The solid segments contain admissible solutions. Pluses, squares and gray circles connected by dashed lines mark the points corresponding to non-admissible solutions that violate the inequalities (16) at $n = 0, 1$ and 2, respectively.

have been obtained for the motion of two screw dislocations on the same slip plane (Flytzanis et al., 1974, Figs. 4 and 5). For given V and for a given

branch of the relation, we can determine μ as the integer part of α: $\mu = \lfloor \alpha \rfloor$. Substituting $\alpha(V)$ along each branch in (50), we obtain the driving force G as a function of V. The first four branches of $G(V)$ at $\chi = 1$ are shown in Fig. 6. Note, along each branch, solutions with sufficiently low and high velocity were

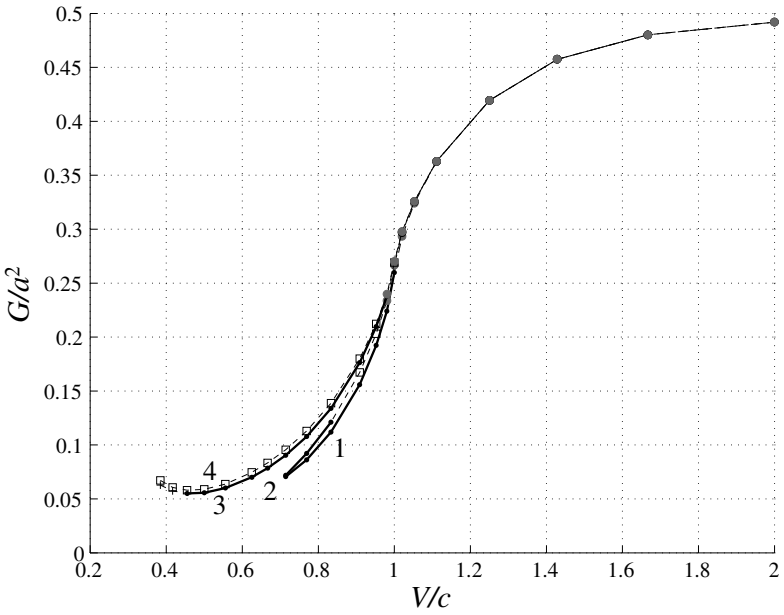

Fig. 6. The first four branches of the kinetic relation $G(V)$ at $\chi = 1$. The solid segments contain admissible solutions. Pluses, squares and gray circles connected by dashed lines mark the points corresponding to non-admissible solutions that violate the inequalities (16) at $n = 0, 1$ and 2, respectively.

excluded since they violated the constraints (16). In some cases, the whole branch becomes non-admissible. Our calculations show that solutions break down in three different ways, with the inequalities (16) violated at $n = 0$, $n = 1$ and $n = 2$ (see Fig. 7). The corresponding points are connected by dashed lines and marked by pluses (failure at $n = 0$), squares ($n = 1$) and gray circles ($n = 2$) in Figures 5 and 6. Note that $n = 2$ failure mode may be preceded or followed by the failure at $n = 1$, but the markers indicate the failure at the highest n. Note that while the driving force G becomes single-valued in the supersonic regime, the relation $\alpha(V)$ remains multivalued for all velocities. The multivaluedness of the kinetic relations means that for a given driving force, multiple solutions with alternate step motion coexist. Some of these solutions, however, can be unstable, and this issue will be explored numerically in Part II of this paper.

To investigate the effect of elastic anisotropy, we consider $\chi \neq 1$. Kinetic relations at $\chi = 0.5$ and $\chi = 2$ are shown in Figs. 8 and 9, respectively. All the non-admissible solutions are depicted in dashed line and valid parts in dotted solid line. Observe that at higher χ, the same velocity can be obtained at lower driving force but the steps have a larger separation between them.

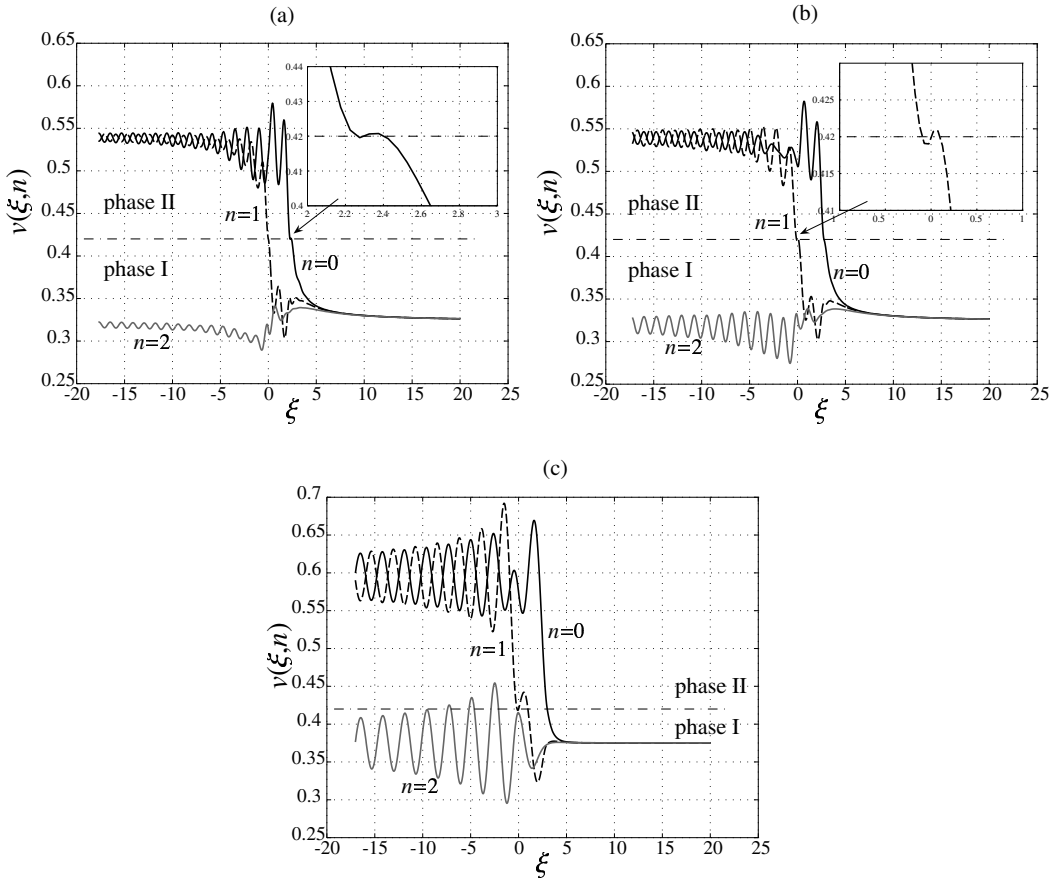

Fig. 7. Examples of non-admissible solutions caused by oscillations violating the inequalities at (a) $n = 0$ ($V/c = 0.4167$, $\alpha = 2.2928$), (b) $n = 1$ ($V/c = 0.5$, $\alpha = 2.7622$) and (c) $n = 1$ and $n = 2$ ($V/c = 1.0204$, $\alpha = 2.9891$). In all examples $\chi = 1$, $v_c = 0.42$ and $a = 0.22$.

Note also as χ decreases, the threshold value of driving force below which the alternate motion is not possible becomes larger.

4.2 Admissible strain profiles

We now consider typical strain profiles generated by the alternate step motion. As before, we restrict our attention to velocities above the first resonance. Fig. 10 shows the strain profiles along the two steps in terms of ξ for the case of $G/a^2 = 0.18$ ($v_- = 0.57$) and $\mu = 1$. From the kinetic curves in Figs. 5 and 6, one can see that this corresponds to $V/c = 0.94$ (subsonic speed) and $\alpha = 1.587$.

Recalling that $v_{m,n}(\tau) = v(m - V\tau, n)$, we can also plot $v_{m,n}(\tau)$ across each step for given τ. Such a plot is shown in Fig. 11. One can see that the moving steps radiate lattice waves. At velocities above the first resonance ($V > V_1^-$)

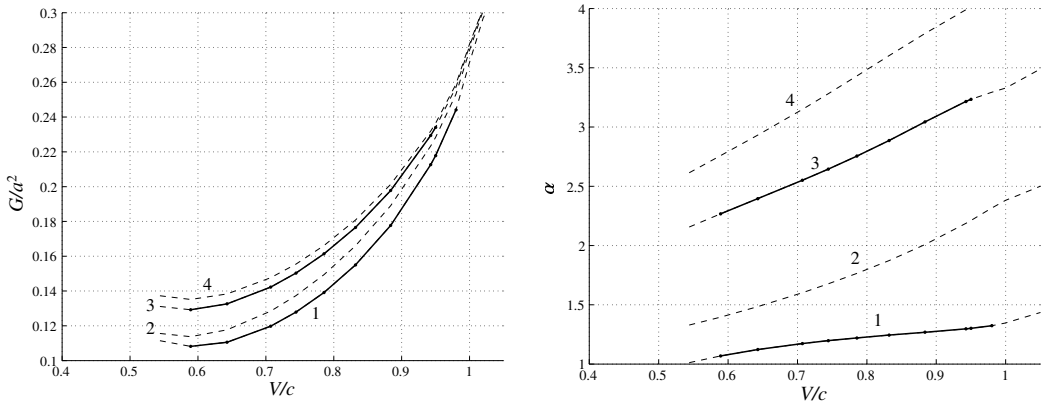

(a) G/a^2 versus V/c (b) α versus V/c

Fig. 8. The first four branches of the kinetic relations $G(V)$ and $\alpha(V)$ at $\chi = 0.5$. The solid segments contain admissible solutions.

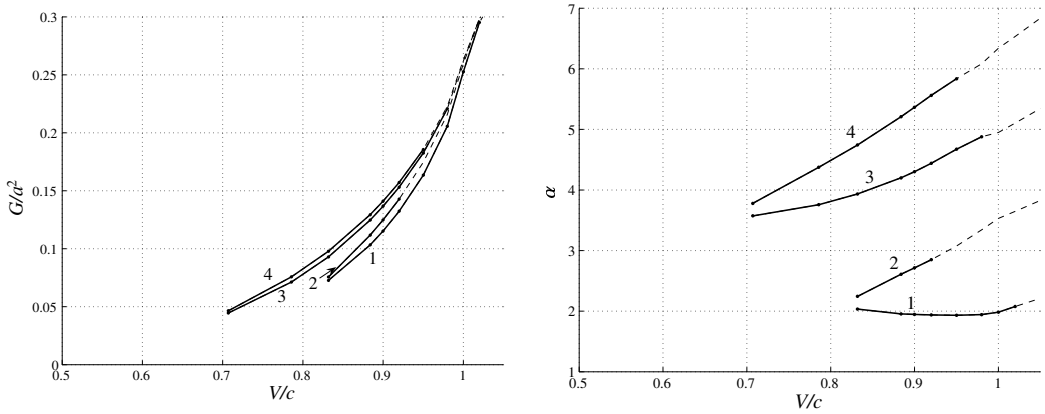

(a) G/a^2 versus V/c (b) α versus V/c

Fig. 9. The first four branches of the kinetic relations $G(V)$ and $\alpha(V)$ at $\chi = 2$. The solid segments contain admissible solutions.

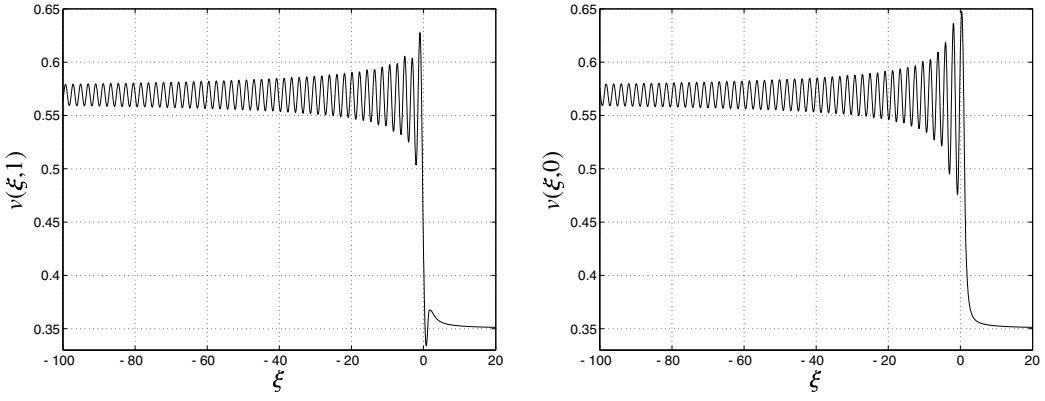

(a) $v(\xi, 1)$ (step #2) (b) $v(\xi, 0)$ (step #1)

Fig. 10. Strain profiles in the moving frame for a subsonic two-step configuration with $G/a^2 = 0.18$ ($v_- = 0.57$), $V/c = 0.94$, $\alpha = 1.587$. The other parameters are $\chi = 1$, $a = 0.22$, $v_c = 0.42$.

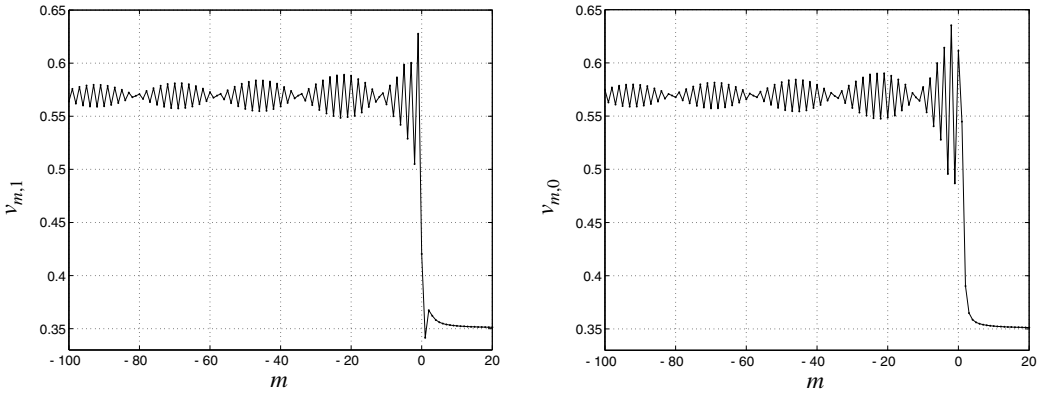

(a) $v_{m,1}(0+)$ (step #2) (b) $v_{m,0}(0+)$ (step #1)

Fig. 11. Snapshots of the strain profile for a subsonically moving two-step configuration in the stationary frame at $\tau = 0+$. The parameters are the same as in Fig. 10.

considered here, the lattice waves appear only behind the moving front. For lower velocities, radiation of waves both behind and in front of the moving steps is expected. Note also that unlike the one-dimensional case (Truskinovsky and Vainchtein, 2005b), where the magnitude of the oscillations does not decay, in the two-dimensional lattice model considered here the amplitude of the lattice waves decreases as $|\xi|^{-1/2}$ inside the wake zone and as $|\xi|^{-1/3}$ along its boundary. See Appendix B for more details.

The distinct beat structure of the lattice waves behind the moving boundary in Fig. 11 is due to the sampling effect, which takes place when the function $\cos(kx)$ has a wave number k close to (but not equal to) π and x is restricted to integer values. Using equations (41) and (42) and the asymptotic expressions for $g_0(\xi)$ and $g_1(\xi)$ derived in Appendix B, one can show the following asymptotic behavior of strains for a subsonic solution behind the moving front ($\xi << -1$):

$$
\begin{aligned}
v(\xi,0) \approx & v_- + \frac{a\sqrt{\chi - V^2}}{2\pi}\left(\frac{1}{\xi} + \frac{\xi}{\xi^2 + (\chi - V^2)}\right) - a\sqrt{\frac{2}{\pi}}\Big(q_0(\xi - \alpha) + q_1(\xi)\Big), \\
v(\xi,1) \approx & v_- + \frac{a\sqrt{\chi - V^2}}{2\pi}\left(\frac{1}{\xi} + \frac{\xi}{\xi^2 + (\chi - V^2)}\right) - a\sqrt{\frac{2}{\pi}}\Big(q_0(\xi) + q_1(\xi - \alpha)\Big), \\
q_0(\xi) = & \frac{2\cos(k_-(\xi) + \frac{\pi}{4})}{k_-\sqrt{|\lambda'(k_-)\xi|}}, \\
q_1(\xi) = & \frac{\lambda(k_+^s) - 1}{k_+^s}\sqrt{\frac{|\xi|}{|\lambda'(k_+^s)||\lambda(k_+^s)\xi^2 + \lambda''(k_+^s)|}}\cos(k_+^s\xi - \frac{\pi}{4} - \theta_+) \\
& + \frac{\lambda(k_-^s) - 1}{k_-^s}\sqrt{\frac{|\xi|}{|\lambda'(k_-^s)||\lambda(k_-^s)\xi^2 + \lambda''(k_-^s)|}}\cos(k_-^s\xi + \frac{\pi}{4} - \theta_-),
\end{aligned}
\tag{51}
$$

where k_- is the root of $\lambda(k_-) = -1$, and $\theta_\pm$ ($0 < \theta_- < \theta_+ < \pi$) solve $\xi \sin\theta_\pm = \lambda'(k_\pm^s)$. Here $k_\pm^s$ satisfy $\lambda(k_\pm^s) = -\cos\theta_\pm$. When k_- is close to π, the beats phenomenon occurs. Substituting $k = \pi$ and $\lambda = -1$ into Eq. (26), we find that the corresponding velocity V must be close to $V_b \approx 2\sqrt{1+\chi}/\pi$ but not equal to this value. At $\chi = 1$ this yields $V/c \approx 0.9$, which is the case in Fig. 11.

More generally, one can use the asymptotic approximations of $g_L(\xi)$ obtained in Appendix B to predict the structure of lattice waves behind the moving front. To demonstrate this, we compare in Fig. 12 the semi-analytical (dotted line) and asymptotic (solid line) values of $g_1(\xi)$ at $\chi = 1$ and $V/c = 0.9395$. The agreement is excellent for sufficiently large $|\xi|$, and similar agreement

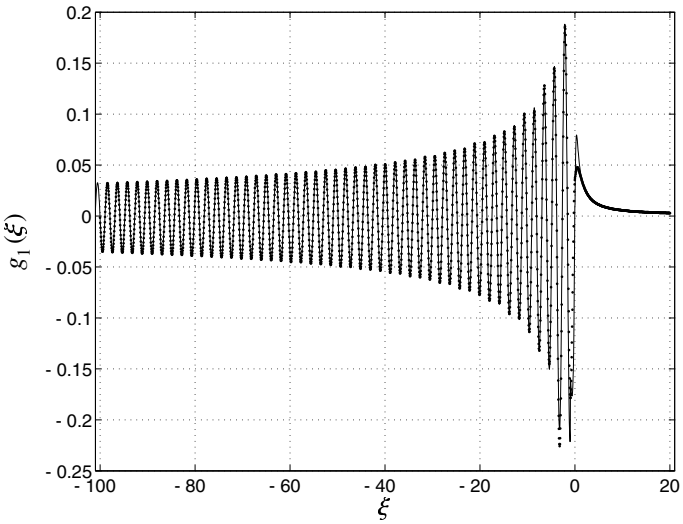

Fig. 12. Comparison of semi-analytical (dotted line) and asymptotic (solid line) values of $g_1(\xi)$. The parameters are $\chi = 1$ and $V/c = 0.9395$.

can be shown for other $g_L(\xi)$. Hence at any point away from the step zone, one can use the asymptotic expressions for $g_L(\xi)$ to obtain the whole solution with the motion parameters satisfying the kinetic relations. Figure 13 depicts a snapshot for a two-step configuration. In order to show the structure of the lattice waves emitted by the moving steps more clearly, only the dynamic part of the strain

$$v_{m,n}^D(\tau) = \sum_{p=0}^{N-1} v_p^D(m - V\tau, n) \tag{52}$$

is plotted.

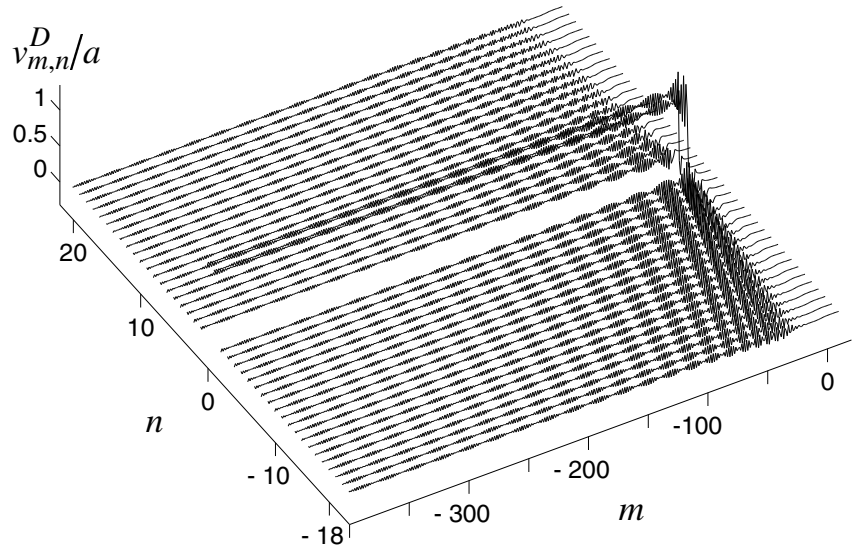

Fig. 13. Snapshot of the asymptotic approximation of the dynamic part of the vertical strain (defined in Eq. (52)) at $\tau = 0+$ showing the structure of the lattice waves emitted by the moving steps. The parameters are $a = 0.22$, $v_c = 0.42$, $v_- = 0.57$, $\chi = 1$, $V/c = 0.9395$ and $\alpha = 1.5829$.

5 Sequential motion of three steps

Consider now a phase boundary with three steps ($N = 3$). In this case the vertical strains along the lines containing the three steps are

$$\begin{aligned} v(\xi,1) =& v_+ + a(g_0(\xi) + g_1(\xi-\alpha_1) + g_2(\xi-\alpha_2)),\\ v(\xi,0) =& v_+ + a(g_1(\xi) + g_0(\xi-\alpha_1) + g_1(\xi-\alpha_2)),\\ v(\xi,-1) =& v_+ + a(g_2(\xi) + g_1(\xi-\alpha_1) + g_0(\xi-\alpha_2)). \end{aligned} \tag{53}$$

Here g_0 and g_1 are given by (43) and (44), respectively, and

$$g_2(\xi) = \frac{1}{2\pi}\int\limits_{-\infty}^{\infty}\left(\frac{(2\lambda^2-1)F(\lambda)-(2\lambda-1)}{ik_\xi}\right)e^{-ik_\xi\xi}\mathrm{d}k_\xi. \tag{54}$$

The system (36) in this case reduces to

$$g_1(-\alpha_1)+g_2(-\alpha_2) = g_1(\alpha_1)+g_1(\alpha_1-\alpha_2) = g_2(\alpha_2)+g_1(\alpha_2-\alpha_1) = \frac{1}{2}-\frac{G}{a^2}-g_0(0). \tag{55}$$

Solution of the first two equations for $\chi = 1$ complying with the constraints (16) is shown in Fig. 14, and its projection onto the plane $\alpha_1 = 0$ is depicted in Fig. 15(a). Fig. 15(b) shows the driving force as a function of V/c and $\alpha_2-\alpha_1$, the separation between second and first steps.

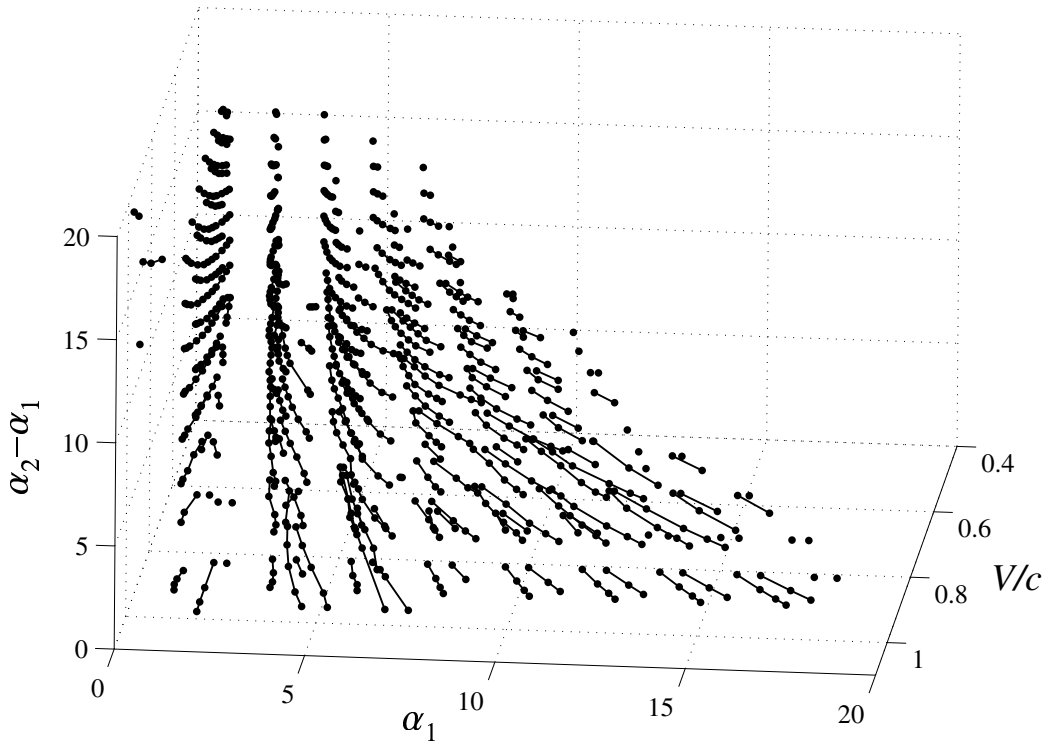

Fig. 14. The separation $\alpha_2 - \alpha_1$ between the first and second steps (in ξ space) versus the separation α_1 between the second and third steps and V/c. Here $\chi = 1$.

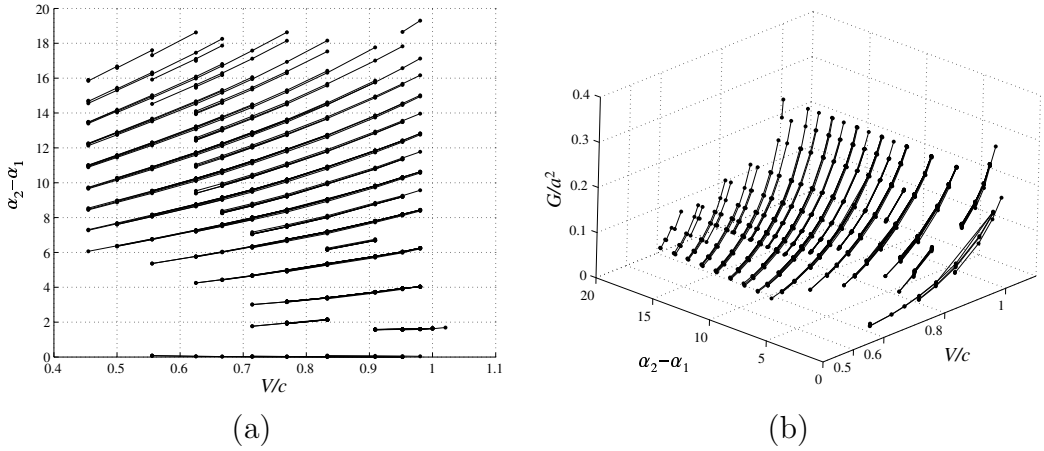

(a) (b)

Fig. 15. (a) The projection of Fig. 14 onto the plane $\alpha_1 = 0$. (b) The driving force G/a^2 versus V/c and $\alpha_2 - \alpha_1$, the separation between the first and second steps. Here $\chi = 1$.

Note that similar to the two-step case, in the three-step configuration the supersonic parts of branches with sufficiently large separation $\alpha_2 - \alpha_1$ between the first two steps are missing since the corresponding solutions violate the constraints (16).

For a multi-step configuration, one may find kinetic relations in a similar manner, but with more complicated equations for the separations. One can

show that the function $\mathcal{S}(L, k_\xi)$ in the definition (34) of $g_L(\xi)$ can be written as

$$\mathcal{S}(L, k_\xi) = a_L(\lambda)F(\lambda) - b_L(\lambda), \qquad L = 0, 1, \ldots, \tag{56}$$

where the coefficients $a_L(\lambda)$ and $b_L(\lambda)$ satisfy the following recurrence relations:

$$\begin{aligned} &a_0 = 1, \qquad b_0 = 0, \\ &a_1 = \lambda, \qquad b_1 = 1, \\ &a_{L+1} = (2\lambda + 1)a_L - (\lambda + 1)b_L, \quad L = 1, 2, \ldots, \\ &b_{L+1} = 2a_L - b_L, \quad L = 1, 2, \ldots. \end{aligned} \tag{57}$$

6 Breakdown of the steady step motion

Kinetic relations in Sections 4.1 and 5 clearly show that the steady sequential propagation of steps exists within certain velocity intervals $[V_L, V_H]$. The velocity bounds V_L and V_H depend on χ and the particular solution branch. When the propagation speed is beyond the velocity range, the solution breaks down because the inequalities (16) no longer hold. It is found that these constraints are violated in two different ways. At low velocities, $V < V_L$, the solution breaks down because the oscillations ahead of the front force some bonds in front of one or more steps to switch to phase II, thus violating the first inequality in (16). An additional breakdown mechanism is observed at high velocities ($V > V_H$). In this case, the large amplitude of waves propagating behind the front causes the bonds directly above the upper step to switch from phase I to phase II, which violates the second inequality in (16). As will be shown in Part II, this results in nucleation of new islands of phase II on top of the upper step. In what follows, we focus on the high-velocity breakdown of steady step propagation and its parameter dependence, leaving the low-velocity breakdown for a future study. For simplicity, we only consider the single-step and two-step configurations.

We first show the upper velocity bound for the steady propagation of a single step. In this case the kinetic relation and solution do not depend on α, and the critical velocities for different values of anisotropy parameter χ can be easily determined. The results of V_H/c are shown in Table 1.

Table 1
The upper velocity bound with different χ for a single-step configuration.

χ	0.5	1	2	4
V_H/c	0.9658	0.9908	0.9994	1.0036

Note that V_H/c increases with higher χ from subsonic to sonic and supersonic values. This implies that if the harmonic horizontal bonds are sufficiently strong, the island nucleation takes place only in the supersonic regime, and the steady supersonic propagation of the step becomes possible at $V < V_H$. This is interesting in view of the close connection with dislocation motion and the recent discussions about whether a dislocation can move supersonically (Gumbsch and Gao, 1999; Rosakis, 2001). Note that the screw dislocation model considered in Ishioka (1971) and Celli and Flytzanis (1970) precludes this possibility, as does the Frenkel-Kontorova model studied in Earmme and Weiner (1973, 1974), where breakdown of the steady dislocation motion at $V/c \approx 0.94$ (0.95 is predicted by Flytzanis et al. (1974)).

For weaker harmonic bonds ($\chi < 2$), the critical speed V_H is subsonic, as in the aforementioned dislocation literature, so that the nucleation takes place already in the subsonic regime. Note, however, that the critical speed we obtained here for the case comparable to the literature ($\chi = 1$) is much closer to the sound speed than the above predictions for a dislocation, for the following reason. Ishioka (1971) and Celli and Flytzanis (1970) used a bilinear periodic potential, so that the relative displacement in the bonds behind the dislocation is constrained from both above and below. Hence sufficiently large oscillations behind the moving front violate the upper limit of this constraint, enabling the formation of another dislocation on the same slip plane (Flytzanis et al., 1974). In contrast, the non-periodic potential employed here to model phase transitions does not constrain the strain in phase II from above, eliminating this possibility and delaying the breakdown of steady motion. Instead, the large magnitude of lattice waves at $V > V_H$ forces the bonds directly *above* the step to change phase. This is equivalent to a new dislocation nucleating on the neighboring slip plane, as envisioned by Ishioka (1975). This indicates that different well structure in the two models leads to different breakdown mechanisms.

Consider now the alternate motion of two steps. Since multiple solutions may exist for the same velocity, the upper velocity bound depends on the solution branch. Table 2 lists these bounds for the first four branches. At small separations (first solution branch) solutions fail, as in the single-step case, due to nucleation of new phase on top of the upper step. At intermediate separation between the two steps (branches 2 and 3 in the table) the constraint (16) may fail at $n = 1$ (ahead of the upper step and on top of the lower one) prior to its failure at $n = 2$ (on top of the upper step). The corresponding values are marked with an asterisk in Table 2. The different mode of failure in this case is due to the waves emitted by the lower step. Recall that the amplitude of these waves increases with velocity. Sufficiently large wave amplitude may cause phase change ahead of the upper step. Note that this can only occur when the step separation is larger than the half wave length of the oscillations emitted by the lower step. At the same time, the amplitude of waves propa-

gating behind the upper step also increases with velocity. When the steps are sufficiently far apart, the waves on top of the upper step have larger amplitude than the waves in front of it, and the breakdown is again due to island nucleation at $n = 2$ (see Fig. 5 and branch 4 at $\chi = 2$ and 4 in Table 2).

Table 2
The upper velocity bounds for the first four branches of solutions for a two-step configuration. The values at which the inequalities (16) fail at $n = 1$ are marked with asterisk. All other critical velocities correspond to failure at $n = 2$.

branch	χ	0.5	1	2	4
1	V_H/c	0.99	1.01	1.02	1.02
2		–	0.85*	0.93*	0.96*
3		0.95*	0.98*	0.99*	0.995*
4		–	–	0.975	0.985

From Table 2 one can see that in the two-step configuration V_H/c also increases with higher χ. In addition, the average critical velocity for steady motion of two steps is slightly higher than those for the single-step configuration. As the separation between the steps increases for given χ, V_H gradually decreases. Note also that the velocity intervals where solutions are valid are more narrow or even non-existent for even-numbered branches. As we will see in Part II, admissible solutions along even-numbered branches are likely unstable.

7 Summary and discussion

In this work, we adopt an anti-plane shear lattice model to study the motion of a finite number of steps along a phase boundary in a crystalline solid undergoing a displacive phase transformation. We assume a steady sequential motion of the steps under an external loading and obtain explicit solutions describing this motion in terms of certain integrals. For the case of sufficiently large velocity, we evaluate the integrals numerically and show that the moving steps emit lattice waves propagating behind the front. The asymptotic expressions of these oscillations are also obtained.

Our analysis also yields kinetic relations between the velocity of the steps, the driving force and the characteristic motion parameters. These are studied in detail for the two-step and three-step configurations. Our results show that multiple solutions exhibiting sequential step motion may exist for a sufficiently large velocity. Numerical simulations described in the second part of this paper suggest that some of these solutions are stable.

The obtained solutions cease to exist outside certain velocity ranges. The high-velocity solution breakdown leads to the nucleation of new islands of bonds of the high-strain phase on top of the existing step configuration. This is verified by numerical simulations in Part II.

The effect of anisotropy is studied by introducing the parameter χ which measures the relative strength of elastic bonds in the direction along the step propagation with respect to the bonds perpendicular to it. We show that at higher χ the steps can move at the same velocity at lower applied loading and are spaced further apart. Another important effect of anisotropy is that the critical speed above which the island nucleation occurs may be either below or above the sound speed. For low enough χ the critical speed is subsonic, leading to a nucleation in the subsonic regime. Meanwhile, at sufficiently large χ the critical speed is slightly above the sonic limit, so that steady supersonic motion becomes possible. In either case, supersonic velocities above the critical value lead to island nucleation. These results are confirmed in Part II, where an independent numerical simulation is conducted.

Acknowledgements

This work was supported by the NSF grant DMS-0443928 (A.V.).

A The driving force for phase boundary propagation

The lattice dynamics studied in this paper is Hamiltonian, so that the energy is conserved on the lattice level. However, the transfer of energy from long waves to short-wave lattice waves emitted by the moving steps results in what is perceived on the macroscopic level as energy dissipation. To compute the rate of macroscopic dissipation, consider a strip of lattice $m_1 \le m \le m_2$ that at time $\tau = \tau_0$ includes the moving N-step front. During the time interval $[\tau_0, \tau_0 + 1/V]$ each step moves to the right by one lattice spacing, so that every nodal displacement of the strip at $\tau = \tau_0 + 1/V$ takes the value of its nearest left neighbor at $\tau = \tau_0$. It is not hard to see that the change of internal energy $\Delta\mathcal{E}$ is

$$\begin{aligned}\Delta\mathcal{E} = \sum_{n=-\infty}^{\infty} &\left(\frac{1}{2}\dot{u}^2_{m_1-1,n} + \phi_{\rm v}(v_{m_1-1,n}) + \phi_{\rm h}(w_{m_1,n})\right) \\ &-\left(\frac{1}{2}\dot{u}^2_{m_2,n} + \phi_{\rm v}(v_{m_2,n}) + \phi_{\rm h}(w_{m_2,n})\right),\end{aligned} \tag{A.1}$$

where $\phi_{\rm v}(v)$ and $\phi_{\rm h}(w)$ denote the dimensionless densities of energy stored in the vertical and horizontal bonds, respectively. As a part of the full external work done to the system, the external loading F contributes $\mathcal{W}_F$, given by

$$\begin{aligned}\mathcal{W}_F =& F\sum_{m=m_1}^{m_2}\Big((u_{m-1,\infty}-u_{m,\infty})-(u_{m-1,-\infty}-u_{m,-\infty})\Big)\\ =& F\Big((u_{m_1-1,\infty}-u_{m_1-1,-\infty})-(u_{m_2,\infty}-u_{m_2,-\infty})\Big)\\ =& F\sum_{n=-\infty}^{\infty}(v_{m_1-1,n}-v_{m_2,n}).\end{aligned}\tag{A.2}$$

In the limit $m_1\to-\infty$ and $m_2\to\infty$ the kinetic energy terms in Eq. (A.1) vanish along with the contribution due to elastic energy of the horizontal bonds. Meanwhile, in Eq. (A.2), $\mathcal{W}_F$ now contains the full external work. Hence Eqs. (A.1) and (A.2) yield

$$\begin{aligned}&\Delta\mathcal{E}=N\left(\frac{1}{2}v_-^2-a(v_--v_c)-\frac{1}{2}v_+^2\right)=Na\left(v_c-\frac{a}{2}\right)=NF_Ma,\\ &\mathcal{W}=\mathcal{W}_F=NFa.\end{aligned}\tag{A.3}$$

Here we have used Eqs. (14) and (20). The rate $\mathcal{R}$ of the macroscopic energy dissipation is thus given by

$$\mathcal{R}=V(\mathcal{W}-\Delta\mathcal{E})=VN(F-F_M)a.\tag{A.4}$$

At the same time, it can be written as

$$\mathcal{R}=NGV,\tag{A.5}$$

where G is the driving force. Combining (A.4) and (A.5), we obtain the formula (37) for the driving force.

B Asymptotics of strain profiles far away from the step core

In this appendix we use the method of steepest descent to derive the asymptotic behavior of $g_L(\xi)$ defined in Eqs. (34) and (33). Since most admissible solutions are subsonic, we focus on the case $V<c$.

In the region away from the step core ($|\xi|\gg1$), the major contribution to the integral in Eq. (34) is from around the singularities in k_ξ of its integrand, i.e., zeros of the denominator $k_\xi=0$ and the singular branch points. The neighborhood of $k_\xi=0$ gives the continuum (long-wave) part $g_L^c(\xi)$ and the singular branch points contribute an oscillatory short-wave part $g_L^s(\xi)$, i.e.,

$$g_L(\xi)=g_L^c(\xi)+g_L^s(\xi).\tag{B.1}$$

To obtain the continuum part, we introduce a new variable s by setting $\lambda = \cosh s$ and rewrite g_L in terms of s. Expanding the resulting integrand in Taylor series around $s = 0$ ($k_\xi = 0$), we obtain

$$g_L^c(\xi) = \delta_{L,0}\rho(\xi) + \frac{1}{2\pi}\frac{\xi\sqrt{\chi - V^2}}{\xi^2 + (\chi - V^2)L^2}. \tag{B.2}$$

We then derive the short-wave part $g_L^s(\xi)$. Let $k_\pm$ denote the positive real root of $\lambda(k_\xi) = \pm 1$, respectively (as before, we consider the velocity interval $V > V_1^-$, where these equations have one positive real root each in the subsonic regime — recall Fig. 3). Defining θ such that $\cos\theta = -\lambda$, we then have that $k_\xi \in [k_-, k_+]$ corresponds to $\theta \in [0, \pi]$, and $k_\xi \in [k_-, +\infty)$ corresponds to $\theta \in i[0, \infty)$ (the upper half of imaginary axis). Let

$$w(\theta) = -i\left(k_\xi(\theta) - \frac{L}{\xi}\theta\right)\mathrm{sgn}\xi. \tag{B.3}$$

One can show that

$$g_L^s(\xi) \sim (-1)^L \frac{1}{\pi}\Re\left\{\int_C \frac{1 + \cos\theta}{k_\xi \lambda'}\exp(|\xi| w(\theta))\mathrm{d}\theta\right\}, \tag{B.4}$$

where the contour C is shown in Fig. B.1 as a double-arrowed path. Throughout this appendix, prime ($'$), when associated with λ, is used only to denote the derivative with respect to k_ξ.

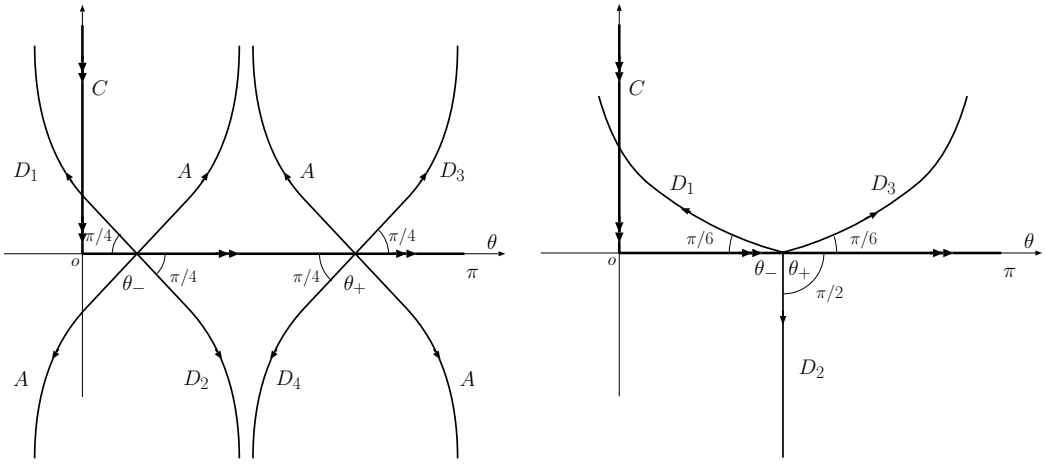

Fig. B.1. Integration contour with (a) well separated, and (b) coinciding saddle points. Here D_i denote the steepest descent directions, and A denotes the ascent directions. In (b), only the descent directions are shown.

From $\cos\theta = -\lambda$, we have $k_{\xi,\theta} = \sin\theta/\lambda^{'}$, and thus

$$w_{,\theta} \equiv \frac{dw}{d\theta} = -i\left(\frac{\sin\theta}{\lambda^{'}} - \frac{L}{\xi}\right)\mathrm{sgn}\xi. \tag{B.5}$$

In the velocity range of interest, both $\lambda^{'}$ and $\lambda^{''}$ are negative around $k_\xi = k_\pm$. Hence $w(\theta)$ has saddle points only when $\xi < 0$ and $|L/\xi|$ is sufficiently small. For a specific L, one can find a critical value of ξ, such that on its two sides the behavior of $g_L(\xi)$ differs essentially. In what follows, we shall call the region of ξ behind such a critical value the wake zone for function $g_L(\xi)$.

We first discuss the case inside the wake zone ($\xi < 0$, small enough $|L/\xi|$). The stationary points of $w(\theta)$ satisfy $\sin\theta = \lambda^{'}(k_\xi(\theta))L/\xi$. Inside the wake zone this equation has two real roots $\theta_\pm$, as shown in Fig. B.1(a). If θ_- and θ_+ are well separated, the correspondent k_ξ are close to $k_\pm$ (and λ are close to ± 1). In addition, at a stationary point θ we have $k_{\xi,\theta\theta} = -(\lambda/\lambda^{'} + (L^2\lambda^{''})/(\xi^2\lambda^{'}))$, hence $k_{\xi,\theta\theta}(\theta_+) > 0$ and $k_{\xi,\theta\theta}(\theta_-) < 0$. Thus $w_{,\theta\theta}(\theta_\pm) = -ik_{\xi,\theta\theta}(\theta_\pm)\mathrm{sgn}\xi$ is nonzero and has an argument of $\pm\pi/4$, respectively. So the steepest descent directions of $\arg(\theta)$ at θ_- are $3\pi/4$ and $7\pi/4$, and the directions at θ_+ are $\pi/4$ and $5\pi/4$. These directions are denoted by D_i, $i = 1, \ldots, 4$, in Fig. B.1(a). The ascent directions are marked by A when shown.

It is then readily seen that the integration contour C can be replaced by $D = (-D_1) \cup D_2 \cup (-D_4) \cup D_3$ up to an asymptotically negligible term. Here and below $-D_i$ denotes the path D_i traversed in the opposite direction. Each contribution of D can be easily calculated (we refer to Bleistein and Handelsman (1975) for the details on the steepest descent method). For $\xi \ll -1$ we then have

$$\begin{aligned} g_L^s(\xi) \sim & \frac{(\lambda-1)}{\pi k_\xi}\sqrt{\frac{2\pi|\xi|}{|\lambda'||\lambda\xi^2 + L^2\lambda''|}}\cos(k_\xi\xi + L(\pi-\theta_+) - \frac{\pi}{4})\Big|_{\theta=\theta_+} + \\ & \frac{(\lambda-1)}{\pi k_\xi}\sqrt{\frac{2\pi|\xi|}{|\lambda'||\lambda\xi^2 + L^2\lambda''|}}\cos(k_\xi\xi + L(\pi-\theta_-) + \frac{\pi}{4})\Big|_{\theta=\theta_-}. \end{aligned} \tag{B.6}$$

The oscillatory part coincides with that given in Celli et al. (1976, formula (4.10)), for a case of a single moving dislocation with a snapping-bond model.

As ξ increases at fixed L, $\theta_+ - \theta_-$ decreases and eventually the two roots merge into a single root θ_0, as shown in Fig. B.1(b). In this case Eq. (B.6) is no longer valid. To obtain the correct result we proceed in the same manner as above and replace C by $D = (-D_1) \cup D_3$, obtaining

$$g_L^s(\xi) \sim \frac{\lambda-1}{\pi k_\xi}\frac{\Gamma(\frac{1}{3})}{\sqrt{3}}\left(\frac{-1}{\lambda'}\right)\left(\frac{6}{|\xi||w^{(3)}(\theta_0)|}\right)^{\frac{1}{3}}\cos(k_\xi\xi + L(\pi-\theta_0)). \tag{B.7}$$

A procedure aiming to obtain the uniform asymptote of $g_L(\xi)$ and utilizing the transformation $w(\theta) = -(t^3/3 - \gamma^2 t) + \beta$ (Bleistein and Handelsman, 1975) gives the following result:

$$g_L^s(\xi) \sim (-1)^L \frac{1}{\pi} \Re \left\{ 2\pi i e^{|\xi|\beta} \left[\frac{a_0}{|\xi|^{\frac{1}{3}}} \mathrm{Ai}(|\xi|^{\frac{2}{3}}\gamma^2) + \frac{a_1}{|\xi|^{\frac{2}{3}}} \mathrm{Ai}'(|\xi|^{\frac{2}{3}}\gamma^2) \right] \right\}, \tag{B.8}$$

where

$$\begin{aligned} \gamma =& i \left| \frac{3}{4}(w(\theta_+) - w(\theta_-) \right|^{1/3}, \qquad \beta = \frac{1}{2}(w(\theta_+) + w(\theta_-)), \\ a_0 =& \frac{G(\gamma) + G(-\gamma)}{2}, \qquad a_1 = \frac{G(\gamma) - G(-\gamma)}{2\gamma}, \\ G(t) =& g(\theta(t)) \frac{d\theta}{dt}, \qquad g(\theta) = \frac{1 + \cos\theta}{k_\xi \lambda'}. \end{aligned} \tag{B.9}$$

Recall that $w(\theta)$ is given in Eq. (B.3). In Eq. (B.8), $\mathrm{Ai}(x)$ is Airy function $\mathrm{Ai}(x) = 1/\pi \int_0^\infty \cos(\tau^3/3 + \tau x) d\tau$, and $\mathrm{Ai}'(x) = d\mathrm{Ai}(x)/dx$. For $d\theta/dt$, we have

$$\begin{aligned} \frac{d\theta}{dt} =& \frac{\gamma^2 - t^2}{w_{,\theta}}, \qquad \theta_+ \neq \theta_- \ (\gamma \neq 0), \ t \neq \pm\gamma, \\ \left.\frac{d\theta}{dt}\right|_{t=\pm\gamma} =& -i \left| \frac{2\gamma}{w_{,\theta\theta}(\theta_\pm)} \right|^{1/2}, \qquad \theta_+ \neq \theta_- \ (\gamma \neq 0), \\ \left.\frac{d\theta}{dt}\right|_{t=0} =& -i \left| \frac{2}{w_{,\theta\theta\theta}(\theta_\pm)} \right|^{1/3}, \qquad \theta_+ = \theta_- \ (\gamma = 0). \end{aligned} \tag{B.10}$$

These are used to determine a_0 and a_1 in Eq. (B.9).

Recalling the asymptotic behavior of $\mathrm{Ai}(x)$,

$$\mathrm{Ai}(x) \sim \begin{cases} \frac{x^{-1/4}}{2\sqrt{\pi}} \exp\left(-\frac{2}{3}x^{3/2}\right), & x \gg 1, \\ \frac{(-x)^{-1/4}}{\sqrt{\pi}} \cos\left(\frac{2}{3}(-x)^{3/2} - \frac{\pi}{4}\right), & x \ll -1, \end{cases} \tag{B.11}$$

and the fact that $\mathrm{Ai}(0) = \sqrt{3}\Gamma(1/3)/(2\pi 3^{2/3})$ and $\mathrm{Ai}'(0) = -1/(3^{1/3}\Gamma(1/3))$, one can verify that the terms of leading order in Eq. (B.8) converge to Eq. (B.6) when θ_- and θ_+ are well separated, and to Eq. (B.7) when they coincide (so that $\gamma = 0$).

We now discuss the case outside the wake zone. Recall that in this case $w(\theta)$ has no saddle points. Instead, we expand $w(\theta)$ in Taylor series up to the third order and expand $g(\theta)$ up to the first order around the reflection point θ_0 such that $w_{,\theta\theta}(\theta_0) = 0$ and substitute the result into Eq. (B.4). We then deduce that Eq. (B.8) still holds if the parameters defined in Eq. (B.9) are replaced

as follows:

$$\gamma = |w_{,\theta}(\theta_0)D|^{1/2}, \qquad \beta = w(\theta_0), \qquad D = -i\left|\frac{2}{w_{,\theta\theta\theta}(\theta_0)}\right|^{1/3}, \tag{B.12}$$
$$a_0 = g(\theta_0)D, \qquad a_1 = g_{,\theta}(\theta_0)D^2.$$

Using (35) together with (B.1), (B.2), (B.6), (B.7) and (B.8), one can show that the conditions (14) at infinity are satisfied.

References

Abeyaratne, R., Vedantam, S., 2003. A lattice-based model of the kinetics of twin boundary motion. J. Mech. Phys. Solids 51, 1675–1700.

Atkinson, W., Cabrera, N., 1965. Motion of a Frenkel-Kontorova dislocation in a one-dimensional crystal. Physical Review A 138 (3), 763–766.

Balk, A. M., Cherkaev, A. V., Slepyan, L. I., 2001a. Dynamics of chains with non-monotone stress-strain relations-I. model and numerical experiments. Journal of the Mechanics and Physics of Solids 49, 131–148.

Balk, A. M., Cherkaev, A. V., Slepyan, L. I., 2001b. Dynamics of chains with non-monotone stress-strain relations-II. nonlinear waves and waves of phase transition. Journal of the Mechanics and Physics of Solids 49, 149–171.

Bhattacharya, K., 2003. Microstructure of Martensite - Why it forms and how it gives rise to the shape-memory effect. Oxford University Press.

Bleistein, N., Handelsman, R., 1975. Asymptotic expansions of integrals. Holt, Rinehart and Winston, New York.

Bray, D., Howe, J., 1996. High-resolution transmission electron microscopy investigation of the face-centered cubic/hexagonal close-packed martensite transformation in Co-31.8 Wt Pct Ni alloy: Part I. Plate interfaces and growth ledges. Metall. Mat. Trans. A 27A, 3362–3370.

Cahn, J. W., Mallet-Paret, J., Vleck, E. S. V., 1998. Traveling wave solutions for systems of ODEs on a two-dimensional spatial lattice. SIAM Journal of Applied Mathematics 59 (2), 455–493.

Capobianco, M., Criscuolo, G., 2003. On quadrature for Cauchy principal value integrals of oscillatory functions. J. Comp. Appl. Math. 156, 471–486.

Carpio, A., Bonilla, L. L., 2003a. Depinning transitions in discrete reaction-diffusion equations. SIAM Journal of Applied Mathematics 63 (3), 1056–1082.

Carpio, A., Bonilla, L. L., 2003b. Oscillatory wave fronts in chains of coupled nonlinear oscillators. Physical Review E 67 (5), 056621.

Carpio, A., Bonilla, L. L., 2003c. Oscillatory wave fronts in chains of coupled nonlinear oscillators. Physical Review B 71 (13), 134105.

Celli, V., Flytzanis, N., 1970. Motion of a screw dislocation in a crystal. J. Appl. Phys. 41 (11), 4443–4447.

Celli, V., Flytzanis, N., Crowley, S., 1976. Analysis of the displacement field of a moving dislocation in a crystal. J. Phys. Chem. Solids 37, 1125–1133.

Chow, S.-N., 2000. Lattice dynamical systems. In: Chow, S.-N., Conti, R., Johnson, R., Mallet-Paret, J., Nussbaum, R. (Eds.), Dynamical Systems. Springer-Verlag, Heidelberg, pp. 1–102.

Christian, J., 1994. Crystallographic theories, interface structures, and transformation mechanisms. Metall. Mat. Trans. A 25A, 1821–1839.

Earmme, Y., Weiner, J., 1973. Can dislocations be accelerated through the sonic barrier? Phys. Rev. Lett. 31 (17), 1055–1057.

Earmme, Y., Weiner, J., 1974. Breakdown phenomena in high-speed dislocations. J. Appl. Phys. 45 (2), 603–609.

Filon, L., 1928–29. On a quadrature formula for trigonometric integrals. Proc. Roy. Soc. Edinburgh 49, 38–47.

Flinn, E., 1960. A modification of Filon's method of numerical integration. J. ACM 7 (2), 181–184.

Flytzanis, N., Celli, V., Nobile, A., 1974. Motion of two screw dislocations in a lattice. J. Appl. Phys. 45 (12), 5176–5181.

Gumbsch, P., Gao, H., 1999. Dislocations faster than the speed of sound. Science 283 (12), 965–968.

Hirth, J., 1994. Ledges and dislocations in phase transformations. Metall. Mat. Trans. A 25A, 1885–1894.

Hirth, J. P., Lothe, J., 1982. Theory of dislocations. John Wiley and Sons.

Iserles, A., Nørsett, S., 2005. Efficient quadrature of highly oscillatory integrals using derivatives. Proc. R. Soc. A 461, 1383–1399.

Ishioka, S., 1971. Uniform motion of a screw dislocation in a lattice. J. Phys. Soc. Jpn. 30 (2), 323–327.

Ishioka, S., 1975. Stress field around a high speed screw dislocation. J. Phys. Chem. Solids 36, 427–430.

Koizumi, H., Kirchner, H., Suzuki, T., 2002. Lattice waves emission from a moving dislocation. Phys. Rev. B 65, 214104.

Kresse, O., Truskinovsky, L., 2003. Mobility of lattice defects: discrete and continuum approaches. Journal of the Mechanics and Physics of Solids 51, 1305–1332.

Kresse, O., Truskinovsky, L., 2004. Lattice friction for crystalline defects: from dislocations to cracks. Journal of the Mechanics and Physics of Solids 52, 2521–2543.

Marder, M., Gross, S., 1995. Origin of crack tip instabilities. Journal of the Mechanics and Physics of Solids 43, 1–48.

Olson, G., Cohen, M., 1979. Interphase-boundary dislocations and the concept of coherency. Acta Metall. 27, 1907–1918.

Papoulis, A., 1962. The Fourier Integral and its Applications. McGraw-Hill Book Company, Inc., New York.

Purohit, P. K., 2002. Dynamics of phase transitions in strings, beams and atomic chains. Ph.D. thesis, California Institute of Technology, Pasadena, California.

Rosakis, P., 2001. Supersonic dislocation kinetics from an augmented peierls model. Phys. Rev. Letters 86 (1), 95–98.

Sharma, B., Vainchtein, A., 2007. Quasistatic propagation of steps along a phase boundary. Continuum Mechanics and Thermodynamics (submitted).

Slepyan, L. I., 1981. Dynamics of a crack in a lattice. Soviet Physics Doklady 26 (5), 538–540.

Slepyan, L. I., 1982. The relation between the solutions of mixed dynamical problems for a continuous elastic medium and a lattice. Soviet Physics Doklady 27 (9), 771–772.

Slepyan, L. I., 2001. Feeding and dissipative waves in fracture and phase transition ii. phase-transition waves. Journal of the Mechanics and Physics of Solids 49, 513–550.

Slepyan, L. I., 2002. Models and phenomena in Fracture Mechanics. Springer-Verlag, New York.

Slepyan, L. I., Ayzenberg-Stepanenko, M. V., 2004. Localized transition waves in bistable-bond lattices. Journal of the Mechanics and Physics of Solids 52, 1447–1479.

Slepyan, L. I., Cherkaev, A., Cherkaev, E., 2005. Transition waves in bistable structures. II. Analytical solution: wave speed and energy dissipation. Journal of the Mechanics and Physics of Solids 53, 407–436.

Slepyan, L. I., Troyankina, L. V., 1984. Fracture wave in a chain structure. Journal of Applied Mechanics and Technical Physics 25 (6), 921–927.

Truskinovsky, L., Vainchtein, A., 2005a. Explicit kinetic relation from "first principles". In: Steinmann, P., Maugin, G. (Eds.), Mechanics of Material Forces. Springer, pp. 43–50.

Truskinovsky, L., Vainchtein, A., 2005b. Kinetics of martensitic phase transitions: Lattice model. SIAM J. Appl. Math. 66 (2), 533–553.

Truskinovsky, L., Vainchtein, A., 2006. Quasicontinuum models of dynamic phase transitions. Continuum Mechanics and Thermodynamics 18, 1–21.

Tsai, H., Rosakis, P., 2001. Quasi-steady growth of twins under stress. J. Mech. Phys. Solids 49, 289–312.

Zhen, Y., Vainchtein, A., 2007. Dynamics of steps along a martensitic phase boundary II: Numerical simulations. Journal of the Mechanics and Physics of Solids (submitted).